TALLINN UNIVERSITY OF TECHNOLOGY
SCHOOL OF ENGINEERING
Department of Materials and Environmental Technology

PHASE EVOLUTION OF $Cu_2CdGeSe_4$ MONOGRAIN POWDERS DURING THE SYNTHESIS PROCESS IN DIFFERENT FLUX MATERIALS

$Cu_2CdGeSe_4$ FAASI KUJUNEMINE MONOTERAPULBRI SÜNTEESI PROTSESSIS ERINEVATES SULANDAJATES

MASTER THESIS

Student name:	Sharath Chandra Pottabathini
Student code:	194227KAYM
Supervisor:	Dr. Marit Kauk-Kuusik Senior Research Scientist
Co-supervisor:	Xiaofeng Li Early State Researcher

Tallinn 2021

(*On the reverse side of title page*)

AUTHOR'S DECLARATION

Hereby I declare, that I have written this thesis independently.
No academic degree has been applied for based on this material. All works, major viewpoints, and data of the other authors used in this thesis have been referenced.

"....." ..... 2021.

Author: .....
/signature /

Thesis is in accordance with terms and requirements

"....." ..... 2021.

Supervisor: .....
/signature/

Accepted for defence

".....".....2021.

Chairman of theses defence commission: .....
/name and signature/

Non-exclusive licence for reproduction and publication of a graduation thesis[1]

I **Sharath Chandra Pottabathini** (author's name)

1. grant Tallinn University of Technology free licence (non-exclusive licence) for my thesis

Phase evolution of $Cu_2CdGeSe_4$ monograin powders during the synthesis process in different flux materials,

(*title of the graduation thesis*)

supervised by Senior Research Scientist, Dr. Marit Kauk-Kuusik,

(*supervisor's name*)

1.1 to be reproduced for the purposes of preservation and electronic publication of the graduation thesis, incl. to be entered in the digital collection of the library of Tallinn University of Technology until expiry of the term of copyright;

1.2 to be published via the web of Tallinn University of Technology, incl. to be entered in the digital collection of the library of Tallinn University of Technology until expiry of the term of copyright.

2. I am aware that the author also retains the rights specified in clause 1 of the non-exclusive licence.

3. I confirm that granting the non-exclusive licence does not infringe other persons' intellectual property rights, the rights arising from the Personal Data Protection Act or rights arising from other legislation.

21.05.2021 (date)

[1] *The non-exclusive licence is not valid during the validity of access restriction indicated in the student's application for restriction on access to the graduation thesis that has been signed by the school's dean, except in case of the university's right to reproduce the thesis for preservation purposes only. If a graduation thesis is based on the joint creative activity of two or more persons and the co-author(s) has/have not granted, by the set deadline, the student defending his/her graduation thesis consent to reproduce and publish the graduation thesis in compliance with clauses 1.1 and 1.2 of the non-exclusive licence, the non-exclusive license shall not be valid for the period.*

Department of Materials and Environmental Technology

THESIS TASK

Student: Pottabathini Sharath Chandra, 194227KAYM (name, student code)

Study programme, KAYM09, Materials, and Processes for Sustainable Energetics

main specialty: Materials for Sustainable Energetics

Supervisor(s): Senior Research Scientist, Dr. Marit Kauk-Kuusik,+372 6203362;

Early-stage researcher, Xiaofeng Li

Thesis topic:

(in English) *Phase evolution of $Cu_2CdGeSe_4$ monograin powders during the synthesis process in different flux materials*

(in Estonian) *$Cu_2CdGeSe_4$ faasi kujunemine monoterapulbri sünteesi protsessis erinevates sulandajates*

Thesis main objectives:

1. Synthesis of $Cu_2CdGeSe_4$ monograin powders in different flux materials such as CdI_2, KI, and LiI.
2. Comparing the phase composition of $Cu_2CdGeSe_4$ monograin powders by Raman analysis, morphology by SEM, and elemental composition by Energy Dispersive X-ray analysis which synthesized in flux materials CdI_2, KI, and LiI.

Thesis tasks and time schedule:

No	Task description	Deadline
1.	Synthesis of $Cu_2CdGeSe_4$ monograin powders in different flux materials such as CdI_2, KI, and LiI	01.10.2020
2.	Analysis of the phase composition (by Raman analysis), morphology(by SEM), and elemental composition (by Energy Dispersive X-ray analysis) of synthesized powder crystals.	01.12.2020
3.	Writing Thesis	20.05.2021

Language: English **Deadline for submission of thesis:** "....."....2021a

Student: Sharath Chandra Pottabathini "....."....2021a

/signature/

Supervisor: Dr. Marit Kauk-Kuusik "....."....2021a

/signature/

Head of study programme: ..... "....."....2021a

/signature/

Terms of thesis closed defence and/or restricted access conditions to be formulated on the reverse side

CONTENTS

PREFACE

This thesis focused on my research topic of Phase evolution during the synthesis process of $Cu_2CdGeSe_4$ monograin powders in different flux materials during the period from 2019 to 2021 in the Laboratory of Photovoltaic Materials at the Department of Materials and Environmental Technology, Tallinn University Of Technology.

I have had the great privilege to work with my supervisor, Senior research scientist Dr. Marit Kauk-Kuusik who has been a very solid and inspiring guide for me. She has put up with my ups and downs and guided me patiently throughout the research process. I thank my co-supervisor Xiaofeng Li (Early state researcher) and special thanks to all members of this research group who have contributed to my thesis: Dr. Kristi Timmo, Dr. Valdek Mikli, Dr. Maris Pilvet, Dr. Mare Altosaar, Dr. Maarja Grossberg, and Fairouz Ghisani (Ph.D. student) who has helped me during my research.

The study was financially supported by the Estonian Research Council grant PRG1023 "Sustainable, cost-efficient, flexible, lightweight and semitransparent multinary chalcogenide-based solar cells for building integrated photovoltaics", by ERDF project „Center of nanomaterials technologies and research (NAMUR+)" (2014-2020.4.01.16-0123) and by the European Regional Development Fund project TK141 "Advanced materials and high-technology devices for sustainable energetics, sensorics and nanoelectronics".

This study analyzes the phase evaluation during the synthesis process of $Cu_2CdGeSe_4$ monograin powders from elemental precursors at multiple temperatures (225, 350, 480, 620, and 700 ^oC) in different molten flux materials CdI_2, LiI, and KI. The synthesized powder crystals surface morphology was analyzed by Scanning Electron Microscopy (SEM), a bulk composition by energy-dispersive X-ray spectroscopy (EDX) and, the phase composition of $Cu_2CdGeSe_4$ powders was analyzed by Raman spectroscopy. At lower temperatures (225 and 350 ^oC) the binary compounds (CdSe, $CuSe_2$) along with ternary compound Cu_2GeSe_3 was noticed. The quaternary compound $Cu_2CdGeSe_4$ started to form from 480 ^oC and showed tetragonal structure by Raman analysis. Some independent peaks are observed for powders synthesized at 620 and 700 ^oC which are not depending on the used flux materials this explains the powders crystallized in orthorhombic structure.

Last but not least, I want to thank my family and friends for their support during my research

List of abbreviations and symbols

CCGSe- $Cu_2CdGeSe_4$

CIGS- $Cu(In,Ga)Se_2$

CIGSSe- $Cu(In, Ga)(S, Se)_2$

CZTS– Cu_2ZnSnS_4

CZTSe- $Cu_2ZnSnSe_4$

CZTSSe- $Cu_2ZnSn(S,Se)_4$

c-Si- Crystalline Silicon

EDX- Energy Dispersive X-ray

HR-SEM- High resolution Scanning Electron Microscope

HT- High temperature

LT- Low temperature

MGL- Monograin layer

o-CCGSe- orthorhombic- $Cu_2CdGeSe_4$

t-CCGSe- tetragonal- $Cu_2CdGeSe_4$

PV- Photovoltaic

SEM- Scanning Electron Microscope

TO- Transverse optical

Keywords: Semiconductor compound, $Cu_2CdGeSe_4$, Solar cells, Molten salts, Phase analysis

INTRODUCTION

Global warming is primarily a climate effect - an increase in the Earth's average surface temperature over the last 150 years. Most of the warming observed on our planet is most likely due to a greenhouse rise, and there is clear evidence that global warming is due to human activities. Most meteorologists and climate scientists say it has been shown that humans affect the phenomena. Many of these environmental effects are caused by energy generation, handling, and usage. The primary cause for environmental effects resulting from the generation, control, and use of resources is that the worldwide use of non-renewable primary energy (oil, coal, natural gas, and nuclear) is a significant factor [1].

The excessive consumption of fossil fuels has increasingly prompted many scientists to conclude that the rise in Earth's surface temperature over decades was attributed to the "Greenhouse Effect" caused by this increase of CO_2 and other gasses in the environment. The effect of the increase is that the carbon dioxide level in the atmosphere is increasing steadily. For both households and industries, solar cells are used to produce electricity as an alternative to conventional fossil fuel power generation. The energy generation from solar technology causes no emission[2].

Silicone (Si), one of the most abundant materials on the Earth's crust, is a semiconducting substance used in the crystalline form (c-Si) for 90% of the PV applications of today. Silicon solar cells are divided based on technology as monocrystalline silicon, multi-crystalline silicon, and amorphous thin-film solar cells. The thin-film solar cells like chalcopyrite's, $Cu(In_xGa_{1-x})Se_2$ (CIGS), and $Cu(In_xGa_{1-x})(S_YSe_{1-y})$ (CIGSSe) were considered as promising alternatives with the high absorption coefficient, tunable bandgap, and doping capacity. It is also a versatile compound that can be generated from stable raw materials using various methods [1]. For CIGS non-vacuum deposition method [3], surface modification by In-S and CIGS absorber layers was formed using physical vapor deposition[4]. The (Ga) and (In) use in CIGS solar cells are rare and expensive materials [5][6]. By substituting the trivalent In/Ga with a bivalent Zn and IV-valent Sn (more abundant materials), we will get Cu_2ZnSnS_4 material. Similarly, also using Cd instead of zinc to get Cu_2CdSnS_4 or replacing Sn by Ge forms Cu_2CdGeS_4 compound [4][7].

Due to unsolved fundamental issues and lack of progress in performance for several years for CZTSSe solar cells, has motivated research on other quaternary copper chalcogenides with suitable bandgap energy for solar cell absorbers. Among them, the $Cu_2CdGeSe_4$ (CCGSe) compound is less studied, although having a *p*-type conductivity and very

promising properties including bandgap energy of about 1.14 -1.29 eV [8]. CCGSe has two crystal structure modifications: a stannite tetragonal structure with a *I-42m* space group (t-CCGSe) and an orthorhombic structure with a *Pmn21* space group (o-CCGSe). The presence of an orthorhombic structure in CCGSe is somewhat different from CZTSSe compounds, where the kesterite structure dominates [8]. In the study [9] was shown that $Cu_2CdGeSe_4$ monograin powder material is possible to synthesize from binary precursors at temperatures 500-700 °C in the liquid phase of CdI_2 and at 700 °C in KI. $Cu_2CdGeSe_4$ powders synthesized at 500 °C had a tetragonal structure and powders synthesized at temperatures 600 °C and 700 °C had orthorhombic structure.

This study analyzes the phase evaluation during the synthesis process of $Cu_2CdGeSe_4$ monograin powders from elemental precursors at multiple temperatures (225 °C, 350 °C, 480 °C, 620 °C, and 700 °C) in different molten flux materials CdI_2, LiI, and KI. The synthesized powder crystals surface morphology was analyzed by Scanning Electron Microscopy (SEM), a bulk composition by energy-dispersive X-ray spectroscopy (EDX) and, the phase composition of $Cu_2CdGeSe_4$ powders was analyzed by Raman spectroscopy in the Laboratory of Photovoltaic Materials, which belongs to the Department of Materials and Environmental Technology, in Tallinn University of Technology.

1. LITERATURE OVERVIEW

1.1 History of photovoltaic cell

The history of photovoltaics (PV) goes back to the nineteenth century. The first functional intentionally made PV device was by Fritts in 1883. He melted Se into a thin sheet on a metal substrate and pressed an Au-leaf film as the top contact. It was nearly 30 cm^2 in the area. The modern era of photovoltaics started in 1954 when researchers at Bell Labs in the USA accidentally discovered that pn junction diodes generated a voltage when the room lights were on. Within a year, they had produced a 6% efficient Si pn junction solar cell. In the same year, the group at Wright Patterson Air Force Base in the US published results of a thin-film heterojunction solar cell based on Cu_2S/CdS also having 6% efficiency [1].

A year later In 1955, Gremmelmaier reported the characteristics of two polycrystalline GaAs solar cells, which had measured efficiencies of 1% and 4% while illuminated with "sea-level sunlight". Gremmelmaier expected a higher efficiency if monocrystalline GaAs were used. This material shows some intrinsic advantages concerning silicon, such as a direct energy gap whose value is well[10]. Thin films of CdTe were also producing cells with 6% efficiency. By this time, the US space program was utilizing Si PV cells for powering satellites. Since space was still the primary application for photovoltaics, studies of radiation effects and more radiation-tolerant devices were made using Li-doped Si [5].

In 1970, a group at the Ioffe Institute led by Alferov (a Nobel laureate), in the USSR, developed a heterophase GaAlAs/GaAs solar cell which solved one of the main problems that affected GaAs devices and pointed the way to new device structures. GaAs cells were of interest due to their high efficiency and their resistance to ionizing radiation in outer space. The year 1973 was pivotal for photovoltaics, in both technical and non-technical areas. A significant improvement in performance occurring in 1973 was the "violet cell" having an improved short wavelength response leading to a 30% relative increase in efficiency over state-of-the-art Si cells. GaAs heterostructure cells were also developed at IBM in the USA having 13% efficiency. In the 1980s, the industry began to mature, as an emphasis on manufacturing and costs grew. Manufacturing facilities for producing PV modules from Si wafer pn junction solar cells were built in the USA, Japan, and Europe[11].

Since 1993, renewable energy technologies such as photovoltaics have been intensively developed in Japan under the "New Sunshine Program" Showa Shell Sekiyu K.K. started to research on the development of $Cu(In,Ga)(Se,S)_2$ (CIGS) thin-film solar cell

technology[12]. They have reached an advanced degree of maturity with proven efficiencies at the laboratory scale beyond 22% [13][14].

The challenge of these materials is to reduce the cost per watt of solar energy conversion. They are formed by expensive and/or scanty elements in the earth's crust such as In, Ga, Te[15]. The following are known to have the most effective semiconductors for future development: $Cu_2ZnSn(S_xSe_{1-x})_4$ (CZTSSe), $Cu_2ZnSnSe_4$ (CZTSe) have kesterite mineral structure and used as light absorbers. In_2S_3 as an alternate buffer layer to conventional CdS. Among the substitute compounds proposed for second-generation solar cells, are the most promising semi-conductors. To achieve an efficient solar cell, it must take into account two conditions associated with light absorber: (a) the efficient absorption of the incident photons to produce electron-hole pairs and (b) the ability to capture the charges produced by the photograph until they recombine. However, the best efficiency achieved in the laboratories for the kesterite-based device was stagnated at 12.6 percent considering the great similarity in composition and crystal structures of CZTSSe and CIGS [16].

The idea of producing solar cells from powder materials is nearly as old as the history of modern silicon-based solar cells [17]. The principal technologies used today for manufacturing solar cells are planar and thin-film technologies. The planar technology is based on the use of very expensive large 3D single crystals. This method of growing large crystals and then cutting them into ultra-thin wafers is therefore not the best way around producing materials. The electronic parameters of the obtained polycrystalline thin-film solid-state solar cells, in general, are much worse than those of monocrystalline solar cells [18].

The development of monograin powder material consists of small crystalline grains and it is possible to prepare the powder in such a way that the crystalline is each physically perfect. In many cases, the chemical composition and the size of the powder grains can also be well controlled. Additional advantages of the developed powder materials besides their single-crystalline structure of every grain are their uniform distribution of doping impurities and a rather narrow granulometric composition. The main feature of monograin layer (MGL) technology is that fabrication of absorber/junction formation and cell/module formation is separated, which leads to several benefits in both stages of MGL production. High temperatures are allowed in adsorber material production, and the possibility of using cheap, flexible, low-temperature substrates allows the production of cheap flexible solar cells [18].

It is possible to achieve uniform distribution of elements due to high synthesis temperatures in the molten phase of flux where the material diffusion and transport process are fast and therefore unwanted secondary phases can be avoided. Unlike the thin film, the material and monograin are prepared separately, enabling to perform post-treatment only on monograins. A flexible cheap substrates can be used enabling versatile could be used as an absorber in the MGL solar cell (Figure 1) [19].

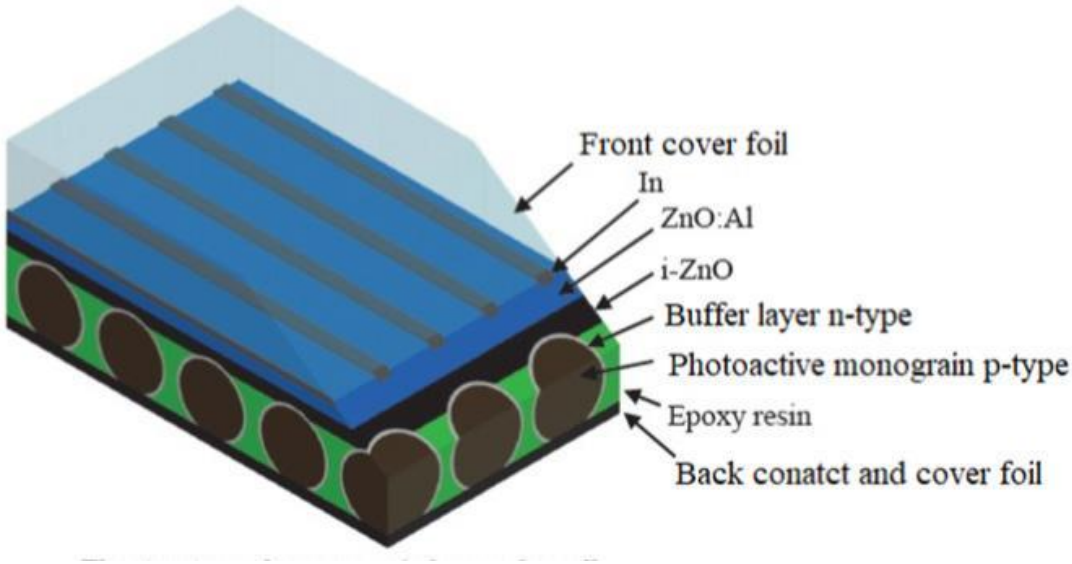

Figure 1. Scheme of the monograin layer solar cell [19]

In developing PV technologies, the performance and costs of the panels have been two big problems and still exist today. There is a general connection between the improvement in productivity and the expense since they usually rise and fall together. For example, the rise in cost due to more costly goods could lead to the same $/W as productivity is improved at the same rate; or the scale effects in manufacturing usually lead to cost savings, assuming the efficiency stays at least the same. However, the cost would not be the most efficient, as each producer is trying to produce the 'supercell' which has high performance and low cost, according to commercial use and market growth. Several cells and modules are required for the optimum solution to different energy systems requirements in terms of cost and performance [1].

1.2 Cu-based quaternary semiconductors for photovoltaic applications

The Cu-based quaternary semiconductor compounds such as Cu_2ZnSnS_4 (CZTS), $Cu_2ZnSnSe_4$ (CZTSe) are earth-abundant and environment-friendly with band gaps between 1.0 and 1.5 eV, very high light absorption coefficient (above 10^5 cm^{-1}), and natural p-type conductivity [20]. These compounds have been intensively studied as low-cost and sustainable solar cell absorber materials. Substituting Cu by another group I (+1 valence) cations, Zn by group II (+2 valence) cations, Sn by group IV (+4 valence) cations, and Sulphur(S) or Selenium (Se) by group VI anions (−2 valence), a class of I_2−II−IV−VI_4 quaternary semiconductors, such as Cu_2ZnGeS_4, $Ag_2CdSnSe_4$, and $Cu_2CdGeSe_4$, can be designed. These quaternary semiconductors have tetrahedrally coordinated crystal structures (derived from zincblende or wurtzite structure) and electronic structure (s−p band gap) similar to the binary II−VI semiconductors (ZnS, CdTe), but their properties are much more diverse given the increased number of elements, so they may have wide applications in electronic, optoelectronic, photovoltaic, or photocatalytic applications [21].

Furthermore, the family of materials generically labeled as "kesterite" due to their structure (CZTSSe) has achieved so far, the highest photovoltaic conversion efficiencies among the emerging CRM (critical raw materials) free technologies, with values in the 11–13% range [22][23]. This family of materials is closely related to the more mature Cu(In, Ga)$(S,Se)_2$ (CIGSSe) technology, already at a commercial stage with reported PV performances comparable to multi-crystalline silicon [24]. The CZTSSe structure is obtained by substitution of two indium (In^{+3}) or gallium (Ga^{+3}) atoms in the CIGSSe structure with one tin (Sn^{+4}) and one zinc (Zn^{+2}) atoms [24]. Additionally, the CZTSSe system can adopt three different structural phases including kesterite, stannite, and disordered kesterite. The kesterite one was demonstrated as the most stable structural polytype [25]. The progress made in the past year's established kesterite as the most relevant and promising CRM-free fully inorganic thin film candidate for large-scale PV deployment to this date [24]. However, due to the relatively low efficiency of kesterite materials compared to conventional PV devices, the researchers are motivated towards the other quaternary copper chalcogenide compound with suitable bandgap energy for solar cell absorbers. Among them, the $Cu_2CdGeSe_4$ compound is less studied, although it has *p*-type conductivity and bandgap energy of about 1.20–1.29 eV [9].

1.3 $Cu_2CdGeSe_4$ properties

1.3.1 Crystal structure

Quaternary chalcogenide compounds based on Cu with the standard Cu_2-B^{II}-C^{IV}-X_4 formula (where B^{II} is Zn, Cd, Hg; C^{IV} is Si, Ge, Sn; X is S, Se) crystallize in tetragonal structures (space group $I\bar{4}\ 2m$ or $I\bar{4}$) and orthorhombic structures (space group $Pmn2_1$, which are derivatives of zincblende or wurtzite cells, with the metals ordered at the cation sites [26][27]. According to [28], the compound $Cu_2CdGeSe_4$ melts incongruously at 831 °C and exhibits a polymorphous transition. It has been determined by X-ray powder and single crystal diffraction that the $Cu_2CdGeSe_4$ compound has two different crystal structures- low- temperature (LT) and high-temperature (HT) modifications. At low temperature 480 °C, the $Cu_2CdGeSe_4$ compound has a tetragonal structure, and at high temperatures 620 and 700 °C, it shows the orthorhombic structure. The determined densities are 5.638 g/cm^3 and 5.7122 g/cm^3 for the orthorhombic HT-$Cu_2CdGeSe_4$ and tetragonal modifications LT-$Cu_2CdGeSe_4$, respectively. In addition to that, lattice parameters of the unit cell for the low-temperature tetragonal structure are reported as a=0.57482(2), c=1.10533(3) nm, and for high-temperature orthorhombic structure the lattice parameters are a=0.80968(9), b=0.68929(6), and c=0.66264(6) nm [28].

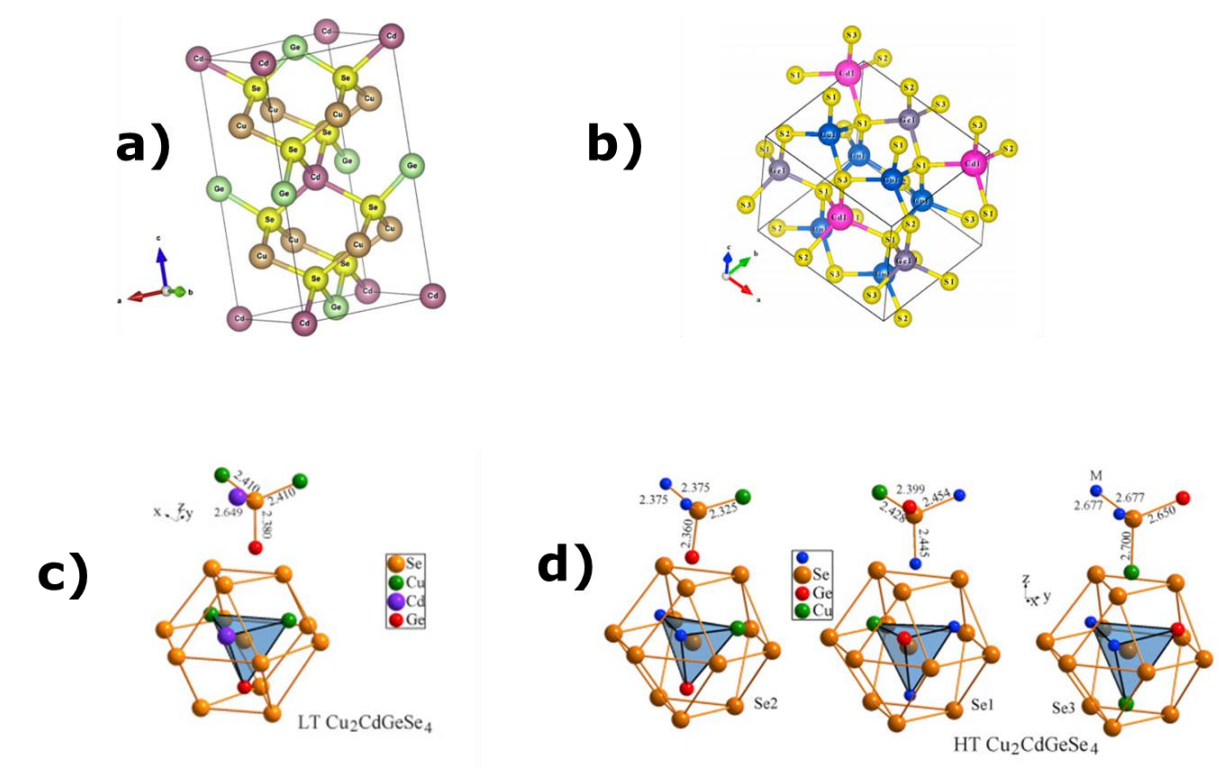

Figure 2: a)Tetragonal structure of LT-$Cu_2CdGeSe_4$ [29], b) HT- $Cu_2CdGeSe_4$ [30], the arrangement of selenium atom at c)LT- $Cu_2CdGeSe_4$ [31], and d)HT- $Cu_2CdGeSe_4$ [31].

Figure 2 shows the crystal structure of a) low- and b) high-temperature modifications of $Cu_2CdGeSe_4$. Usually, it is presented as the packing of selenium tetrahedra centered on germanium atoms [31].

In the case of LT- $Cu_2CdGeSe_4$, the anion sub-lattice forms cuboctahedra, and in the case of HT-$Cu_2CdGeSe_4$, the hexagonal analogs form cuboctahedra. Interatomic distance demonstrates that distances between the metal atoms and selenium atoms are somewhat contracted and that the distances between Se-Se are weak in general concerning the sum of the ionic distances of the elements [31].

In this study, the $Cu_2CdGeSe_4$ compound is synthesized from Cu, CdSe, Ge, and Se precursors. Therefore, the phase diagrams in the system Cu-CdSe-Ge-Se are very important and will be discussed in the following sections.

1.3.2 Phase diagrams

1.3.2.1 Cu-Se phase diagram

According to the study [32], the phase-relations in the Cu-Se system were determined by evacuated silica-tube experiments. From Figure 3, the phase diagram up to 1100 °C was obtained from the results of differential thermal analyses of pure compounds and their mixtures.

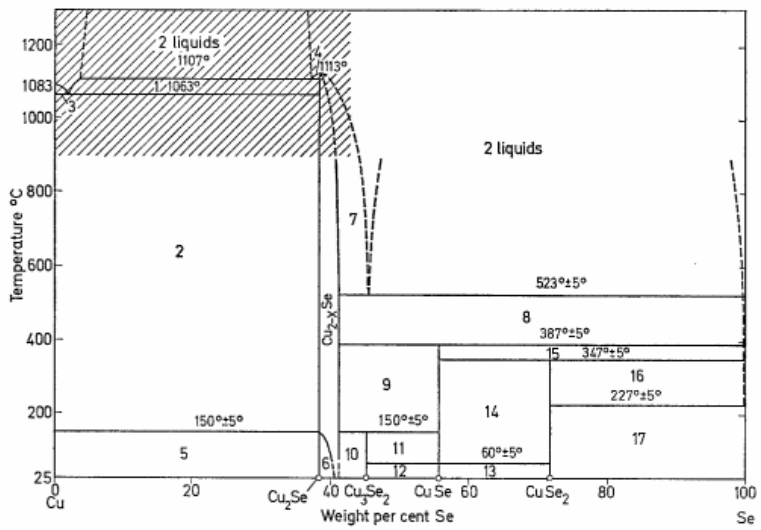

Figure 3: Phase diagram of system Cu-Se- (1) liquid+ β-Cu_2Se; (2) Cu+ β-Cu_2Se; (3) Cu+ Liquid; (4) liquid+$Cu_{2-x}Se$; (5) Cu+α-Cu_2Se; (6) α-Cu_2Se + $Cu_{2-x}Se$; (7) $Cu_{2-x}Se$ + liquid; (8) $Cu_{2-x}Se$ + liquid; (9) $Cu_{2-x}Se$ + CuSe (HT); (10) $Cu_{2-x}Se$+Cu_3Se_2; (11) Cu_3Se_2+CuSe (HT); (12) Cu_3Se_2+CuSe (LT); (13) CuSe (LT)+$CuSe_2$; (14) CuSe(HT)+$CuSe_2$; (15) CuSe (HT)+liquid; (16) $CuSe_2$+liquid; (17) $CuSe_2$ + Se [32].

The phases in the system are shown in Figure 3:

- At point (5), Cu_2Se - undergoes a polymorphic transformation at 150 ° C. The symmetry of the low-temperature form is not yet known. The high-temperature form is cubic with a fluorite-type structure.
- At point (6), $Cu_{2-x}Se$ - cubic, with x variable in a very narrow range, at room temperature.
- At point (11), Cu_3Se_2 - tetragonal, breaks down to $Cu_{2-x}Se$ and CuSe at 150 °C.
- At point (14), CuSe - hexagonal below 60 °C and, presumably, orthorhombic at a higher temperature, melts incongruently at 387 °C to $Cu_{2-x}Se$ and a Se-rich liquid(pt.8)
- At point (15), $CuSe_2$ - orthorhombic, melts incongruently at 347 °C to CuSe and a Se-rich liquid.

The presence of a eutectic at 523 °C was inferred from differential thermal heating and cooling curves.

1.3.2.2 Cu_2Se–CdSe phase diagram

According to the study [33], Figure 4 shows that the $Cu_{1.9}Se$–CdSe diagram is a eutectic type of substantial component with small solubility. The eutectic occurs at 53 mol % CdSe and a temperature of 910 °C. The extent of the Cu_2Se homogeneity range is 50 mol% CdSe at the eutectic temperature and decreases substantially with decreasing temperature (8 mol% Cu_2Se at 602°C). The homogeneity range of CdSe extends to 3.5 mol% Cu_2Se at (900 °C) and 0.4 mol% Cu_2Se at 600 °C.

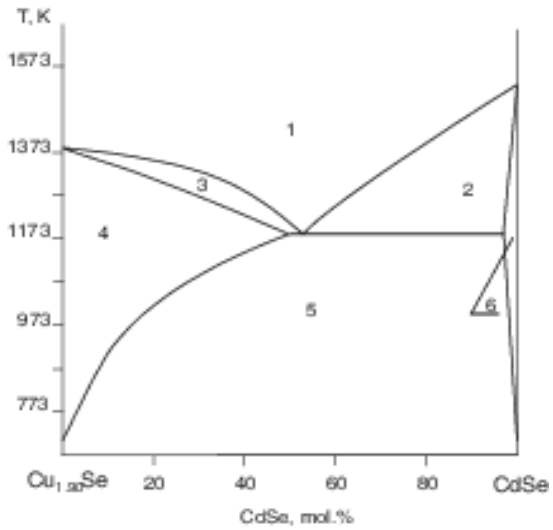

Figure 4: $Cu_{1.9}Se$–CdSe phase diagram- (1) L, (2) L + CdSe, (3) L + $Cu_{1.9}Se$, (4) $Cu_{1.9}Se$, (5) $Cu_{1.9}Se$ +CdSe, (6) CdSe [33]

1.3.2.3 Ge-Se phase diagram

Figure 5 illustrates the phase diagram of Ge-Se. In the system, Ge-Se has observed two stable chemical compounds: GeSe and $GeSe_2$. GeSe melts incongruently at 675 °C and transforms polymorphically from cubic to a low- temperature orthorhombic structure between 666 and 647 °C. $GeSe_2$ with a monoclinic structure melts congruently at 742 °C. The eutectic between α-GeSe and $GeSe_2$ melts at 583 °C and the composition is 56 at.% Se. On the side of the diagram corresponding to a selenium-rich domain, is observed the eutectic reaction: Liquid → $GeSe_2$ + Se. The coordinates of the eutectic point are 182 °C and 94.5 at% Se [34][35].

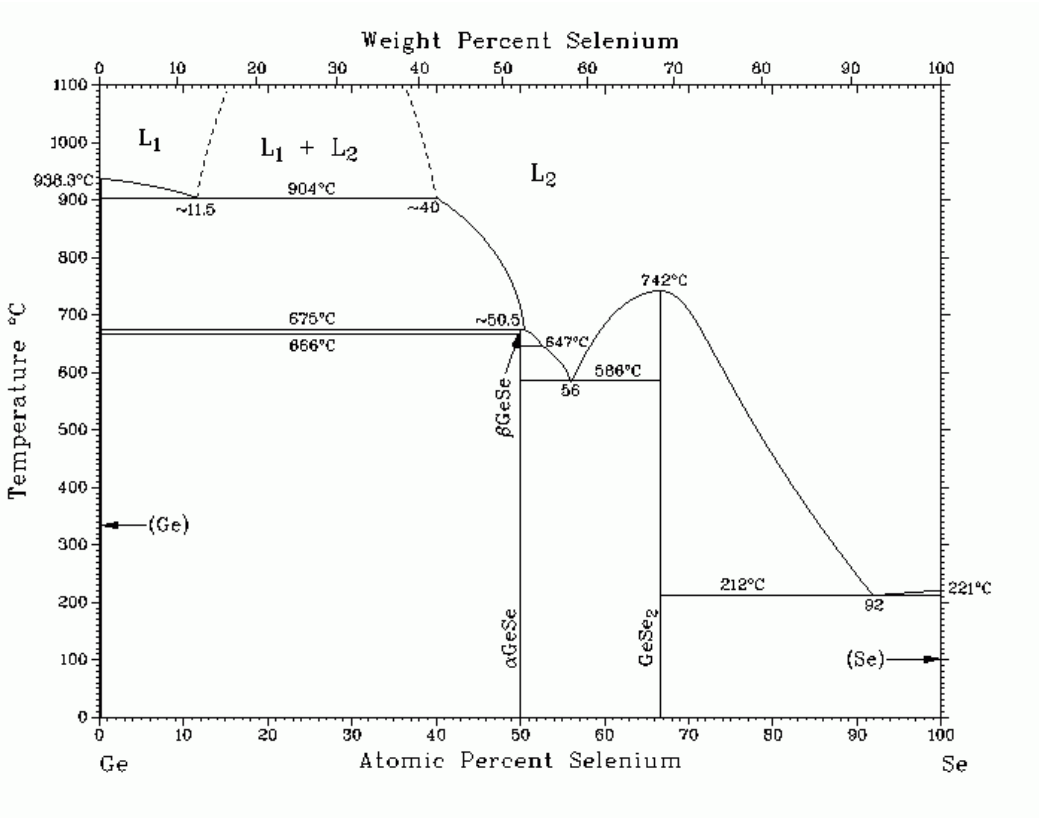

Figure 5: Phase diagram of system Ge-Se [34].

1.3.2.4 Cu_2Se-$GeSe_2$ phase diagram

In the study [36], The physicochemical analysis investigated the phase equilibria in the quasi-ternary Cu_2Se–$GeSe_2$ system. The existence of the below-mentioned contradictions concerning the interaction between the components in the Cu_2Se–$GeSe_2$ system caused its detailed study within the concentration region of 15–60 mol% $GeSe_2$. This research shows that there are two compounds (Cu_2GeSe_3 and Cu_8GeSe_6).

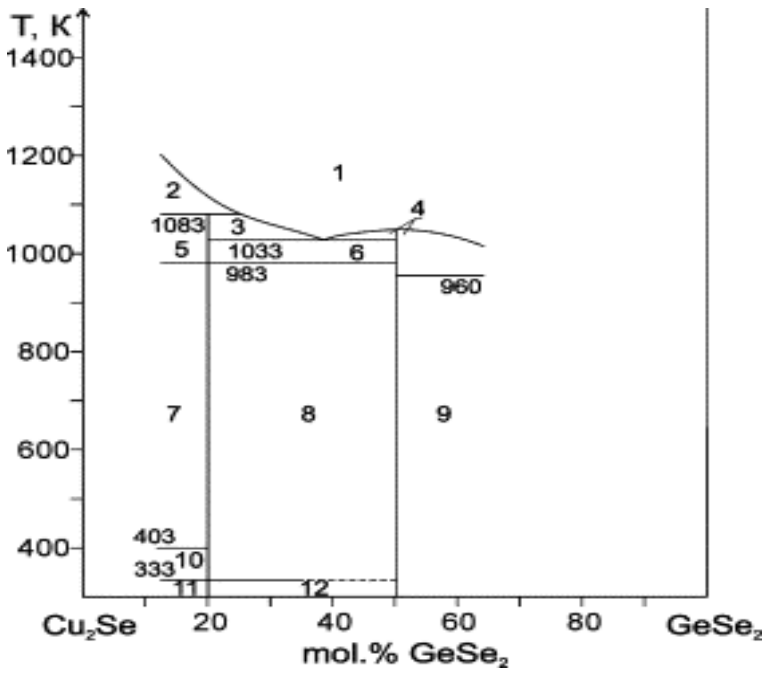

Figure 6: Diagram of phase equilibria in the Cu_2Se–$GeSe_2$ system within the concentration interval of 15–65 mol% $GeSe_2$: (1) L; (2) L+α'-Cu_2Se; (3) L+γ-Cu_8GeSe_6; (4) L+Cu_2GeSe_3; (5) α'-Cu_2Se+γ-Cu_8GeSe_6; (6) γ-Cu_8GeSe_6+Cu_2GeSe_3; (7) α'-Cu_2Se+β-Cu_8GeSe_6; (8) β-Cu_8GeSe_6+Cu_2GeSe_3; (9) Cu_2GeSe_3+$GeSe_2$; (10) α-Cu_2Se+β-Cu_8GeSe_6; (11) α-Cu_2Se+α-Cu_8GeSe_6; (12) α-Cu_8GeSe_6+Cu_2GeSe_3 [36].

The ternary Cu_2GeSe_3 compound melts at 780 °C congruently. Due to the peritectic reaction at 810 °C forms the Cu_8GeSe_6 compound. Two polymorphous transformations occurred at 710 °C and 60°C, respectively. At 131 °C, the horizontal corresponds to the polymorphic transformation of Cu_2Se. The eutectic coordinates are 38 mol% $GeSe_2$ and 780 °C [36].

1.3.2.5 Cu_2GeSe_3–CdSe phase diagram

The phase diagram of the Cu_2GeSe_3–CdSe system is shown in Figure 7. Besides the quaternary $Cu_2CdGeSe_4$ compound, possessing a narrow homogeneity region and forming incongruently at 830 °C, another quaternary phase with the approximate composition $Cu_2Cd_3GeSe_6$ (75 mol% CdSe and 25 mol% Cu_2GeSe_3) was revealed [37]. $Cu_2Cd_3GeSe_6$ forms at 900 °C and decomposes at 736 °C according to the eutectoid reaction $Cu_2Cd_3GeSe_6 \Leftrightarrow Cu_2CdGeSe_4$+CdSe. At 770 °C, the eutectic between $Cu_2CdGeSe_4$ and Cu_2GeSe_3 melts showed in Figure 7 .

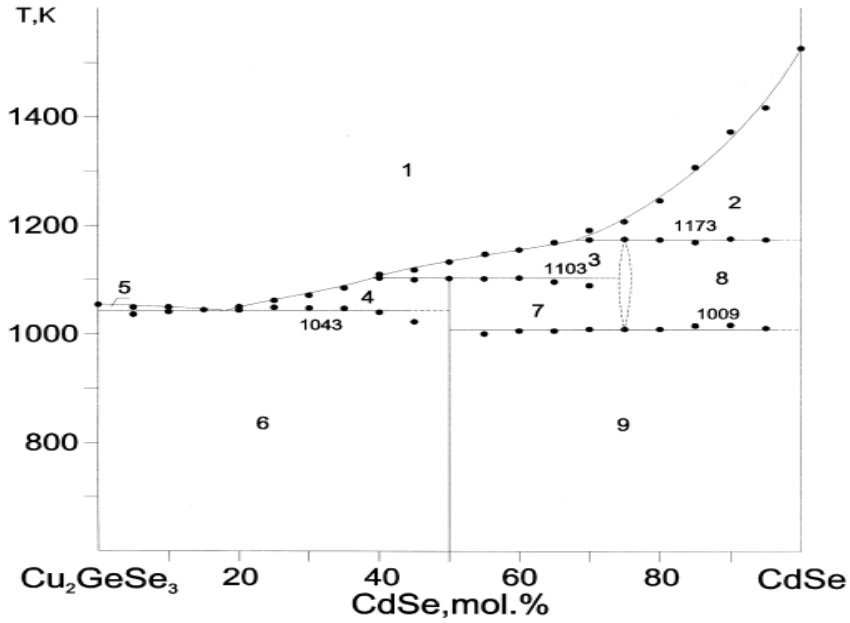

Figure 7: Phase diagram of the quasi-binary section Cu_2GeSe_3–CdSe: (1) L, (2) L+CdSe, (3) L+ $Cu_2Cd_3GeSe_6$, (4) L+$Cu_2CdGeSe_4$, (5) L+Cu_2GeSe_3, (6) $Cu_2CdGeSe_4$+Cu_2GeSe_3, (7) $Cu_2Cd_3GeSe_6$+ $Cu_2CdGeSe_4$, (8) $Cu_2Cd_3GeSe_6$+CdSe, (9) $Cu_2CdGeSe_4$+CdSe [37].

1.4 $Cu_2CdGeSe_4$ synthesis methods

Several reports have been made about $Cu_2CdGeSe_4$ synthesis using various methods such as the horizontal gradient freezing process [38], the Bridgman method [29], and the solid-state reaction method in sealed evacuated quartz ampoules [31]. According to the study [36][38], $Cu_2CdGeSe_4$ has been characterized by the horizontal gradient freezing method from the melts and the primitive optical and electrical properties of single crystals.

According to the study [38], the bulk crystals were grown by using the respective melts' horizontal gradient freezing method (HGF). The weighed material was sealed in a quartz tube and heated for 20 hours at 950–975°C and held 24 hours at the same temperature. At 6 to 10°C/h, the entire region was then cooled electrically, retaining a gradient in temperature of 3°C/cm. By DTA analysis melting point of $Cu_2CdGeSe_4$ was determined to be 840 °C. The electrical resistivities in the range 10^{-2} Ω*cm with the p-type conduction were obtained for $Cu_2CdGeSe_4$. The results showed also that the $Cu_2CdGeSe_4$ compound has a bandgap suitable for optimum conversion efficiency for solar cells (1.2 eV).

A molten salt method has been used in the study [39] to create high-quality $Cu_2CdGeSe_4$ micro-crystalline powder at 700°C. The powder needs additional annealing at 400 °C to improve the performance of the solar cells. According to EDX analysis, the surface of crystals was covered by amorphous selenium. The surface became more Cu-rich and Cd-

poor, as the ratio of [Cu]/ ([Cd] + [Ge]) increased from 0.96 to 1.02. All in all, there were several methods available to synthesize the $Cu_2CdGeSe_4$ compound.

1.4.1 Molten salt synthesis

Molten salts have proven to be useful as alternative reaction media for various organic and inorganic reactions. Single crystals or single-crystalline powders can be obtained at temperatures above the melting point of the used salt at temperatures lower than the melting point of the semiconductor itself. Synthesis in molten salts enhances the rate of solid-state reactions due to the much higher diffusion rates between reaction components in the molten media, lowering the reaction temperature, increasing the homogeneity of the solid product, and controlling the particle size and shape as well as their agglomeration state [25].

In monograin powders, the crystals are formed in the presence of the liquid phase of the used flux salt. The characteristics of monograin crystals are controlled by the selection of the synthesis temperature, as well as the nature and amount of the salt. After the synthesis, the used salt is removed by washing with a suitable solvent and the released monograin powder is dried and sieved. The amount of precursors for the main compound and flux salt is usually taken so that the ratio of the forming volumes of solid-phase V_S and liquid phase V_L is within the range of 0.6–1.0 [25].

In the studies [9][39], $Cu_2CdGeSe_4$ powder materials were synthesized by the molten salt method for photovoltaic applications. Cadmium iodide and potassium iodide were used as fluxes. A major technological advantage of the usage of these salts as flux materials is the possibility to remove them after the growth process very easily by a simple dissolution process in water. Results showed that the $Cu_2CdGeSe_4$ powder crystals synthesized at 500 °C had a tetragonal structure and those synthesized at 600 °C and 700 °C had orthorhombic structure. The bandgap values determined from external quantum efficiency measurements were 1.27 eV for orthorhombic $Cu_2CdGeSe_4$ and 1.14 eV for tetragonal $Cu_2CdGeSe_4$ powder crystals [9]. According to the study [39], the morphology analysis showed that the median size of the crystals increased with lower Cu-content and higher Cd-content in precursors (amount of crystals with diameter > 100 μm increased from 72 to 88% of total weight). According to the EDX results the average bulk composition of all powders was slightly Cu-poor (([Cu]/([Cd]+[Ge]) = 0.96)) and Cd-rich ([Cd]/[Ge] = 1.09) [39]. The monograin layer solar cell on the base of orthorhombic $Cu_2CdGeSe_4$ powder showed the best conversion efficiency of 5.7% [39].

In general, the synthesis of monograin $Cu_2CdGeSe_4$ materials in molten fluxes results in homogeneous materials. The flux material should usually have low melting temperatures and high-water solubility, making it easier to remove the powders from the flux. A variety of flux materials are suitable for the synthesis of monograin powder or recrystallization of these $Cu_2CdGeSe_4$ absorber materials - such as KI, LiI, and CdI_2. Although the phase evolution during the synthesis process and lowest synthesis temperature for homogeneous single-phase $Cu_2CdGeSe_4$ powders growth is not studied.

1.5 Summary of a literature overview and aim of the study

The rise of conventional energy prices has increased the investment attention for renewable energies, in particular photovoltaics, significantly. Thin-film solar cells still offer the possibility of reducing manufacturing costs considerably their component elements are earth-abundant and environment-friendly, their band gaps are close to the optimal bandgap of the light-absorber semiconductor for single-junction solar cells. Quaternary semiconductors (I_2−II−IV−VI_4 with I = Cu, Ag, II = Zn, Cd, IV = Si, Ge, Sn, Pb, and VI = S, Se) have been intensively studied as low-cost and sustainable absorber materials for solar cell. The properties are much more diverse due to the increased number of elements and they have a wide range of applications in electronic, optoelectronic, photovoltaic, or photocatalytic applications. Among them, the $Cu_2CdGeSe_4$ (CCGSe) compound is less studied, although having a p-type conductivity and very promising properties including bandgap energy of about 1.14 -1.29 eV.

The monograin powder technology is one of the methods for the growth of high-quality $Cu_2CdGeSe_4$ absorber materials for solar cells. The quasi-binary phase diagram in section Cu_2GeSe_3–CdSe shows that the $Cu_2CdGeSe_4$ compound melts incongruently at 830 °C and possesses a narrow homogeneity region. Therefore, the formation of $Cu_2CdGeSe_4$ without secondary phases is a challenging task.

It was also found that the $Cu_2CdGeSe_4$ compound exists in two different crystal structures depending on the synthesis temperature- LT- $Cu_2CdGeSe_4$ has a tetragonal structure and the HT- $Cu_2CdGeSe_4$ crystallizes in the orthorhombic structure.

For the synthesis of monograins, the liquid phase of the flux material is an advantage because it enables the quick diffusion of the components through the liquid phase and thus provides a homogeneous composition for multinary compound crystals.

In this thesis, $Cu_2CdGeSe_4$ monograin powders were synthesized in different flux materials such as CdI_2, KI, and LiI. The selection of flux materials was based on their inherent properties- the melting temperature of these salts is lower than the main compound, solubility in water is high and solubility of flux components in a quaternary compound is low. It is known that flux material influences the average particle size and the shape of monograin powders. Also, the quality of the $Cu_2CdGeSe_4$ crystals and formation pathways may vary in different flux materials. Therefore, this study aimed to characterize the phase evolution in the system Cu-CdSe-Ge-Se at multiple temperatures - 225, 350, 480, 620, and 700 ^{o}C in 3 different flux materials- CdI_2, KI, and LiI and find the lowest growth temperatures for homogeneous $Cu_2CdGeSe_4$ monograin powder synthesis in these fluxes.

2. EXPERIMENTAL

In this study, the high purity $Cu_2CdGeSe_4$ monograin powder materials formation in different molten salts were investigated. The monograin powder was synthesized from elemental metal powders Cu, Ge, and Se and binary powder CdSe with a purity of 99.999%. For fluxes, three different salts, CdI_2, LiI with a purity of 99%, and KI with a purity of 99.9% were used. A significant technical advantage of using these salts as flux materials is that these salts can be quickly extracted by a simple water dissolution method after the growth process. The experiment is designed by considering the melting points of elemental powders (Cu=1085 °C[40], Ge=939 °C [40], Se=220 °C [40], CdSe=1240 °C [41]) and the flux materials at multiple temperatures 225, 350, 480, 620, and 700 °C.

- **CdI_2 properties**

In CdI_2, the iodide anions form a compressed hexagonal organization as cadmium cations fill in altered layers of all octahedral sites. A layered lattice comprises the resulting structure. The cadmium iodide is mainly ionically bonded but with a partial covalent character [42]. The melting temperature of CdI_2 is 387 °C, and its boiling point is 742 °C- CdI_2 also has a high solubility in water (approx. 847 g L^{-1} at 20 °C).

- **LiI properties**

LiI is an inorganic compound, which can be in various types of hydrates, namely monohydrate, dehydrate, and trihydrate. Lithium iodide is soluble in water, alcohol, acetone, and methanol. It is very soluble in Ammonium hydroxide. The melting temperature of LiI is 446 °C and boiling point at 1170 °C. Its solubility rate in the water is 1670 g L^{-1} at 25 °C [43].

- **KI properties**

KI is usually a colorless compound, and it can be available as white cubic crystals or in the form of granules. When it is exposed to bright light, it becomes yellowish because of photochemical decomposition traces of iodine. KI has a density of 3.13 g/cm^3, and it melts at 681 °C. KI is highly soluble in water approximately 1400 g L^{-1} at 20 °C. It can also be dissolved in other solutions like iodine and moderately dissolve in ethanol and acetone [44].

2.1 Powder Preparation

The desired amount of monograin powder $Cu_2CdGeSe_4$ was weighed from elemental metal powders Cu, Ge, Se, and binary powder CdSe in a glove box. The total mass of $Cu_2CdGeSe_4$ was equal to the amount of flux material. Three batches of precursor powders were

weighed individually by considering the total amount is approximately 5 grams for the batch. Table 1 explains the considered amount of each precursor powder.

Table 1: Mass parameters of each precursor material in different batches

Precursor material	**Required amount for 5 g of $Cu_2CdGeSe_4$ (g)**	**Batch 1 (g)**	**Batch 2 (g)**	**Batch 3 (g)**
Copper (Cu)	1.01	1.00	1.00	1.00
Cadmium selenide (CdSe)	1.52	1.52	1.52	1.51
Germanium (Ge)	0.58	0.58	0.57	0.58
Selenium(Se)	1.89	1.88	1.89	1.89

After that, the same amount of different flux materials was added to each batch. Later, each batch was divided into five equal parts, shown in Table 2. Samples were named regarding used flux and synthesis temperature (for example CI225 means that powder is synthesized in CdI_2 at 225 °C for 1 week). Each portion of the powder, which is already mixed with the flux material, was put in quartz ampoules, and sealed under vacuum at room temperature. The quartz ampoules were placed into the Split Tube Furnace with separated temperature controllers. Each zone in the furnace was set to different considered temperatures. In each split of the furnace, a maximum of three samples was placed. The maintained temperature of each sample was explained briefly in Table 2. To increase the temperature slowly in the furnace, the temperature increased gradually at one degree per minute. The synthesis action duration for all samples was one week.

Table 2: Mass parameters of each sample with heat treatment duration

Sample name	**Mass of the sample (g)**	**Temperature (° C)**
CI225	1.99	225
CI350	2.00	350
CI480	2.01	480
CI620	2.03	620
CI700	2.01	700
LI225	2.50	225
LI350	1.96	350
LI480	2.02	480
LI620	2.06	620
LI700	2.30	700
KI225	1.99	225
KI350	2.00	350
KI480	2.00	480
KI620	2.00	620
KI700	2.58	700

The synthesis ended by taking samples out of the furnace and fast cooling to room temperature by quenching into the water. The quartz ampoules were opened at one end carefully by cutting them with an electric grinding blade. After opening the ampoules, the synthesized material was separated from each sample by DI water in the ultrasonic bath process. The temperature of water in an ultrasonic bath was set as 50 °C. Each ampoule was placed in a different beaker filled with water until it drowned and placed in an ultrasonic bath for 10 min.

This process is repeated for all other samples until the water becomes transparent. In the end, solid particles were collected in a small beaker by draining all water. The beakers were placed in a hot air thermostat for drying, which is already set as a temperature of 50°C. The dried powder was weighed by high precision lab-scale and noted carefully. Table 3 gives a detailed sample weight of dried powders before and after washing.

Table 3: Before and after synthesis masses of the samples

Sample name	Mass of the sample before synthesis, (g) (precursors+ flux)	Mass of the sample after synthesis, (g) (synthesized powder without flux)
CI225	1.99	0.27
CI350	2.00	0.55
CI480	2.01	0.75
CI620	2.03	0.60
CI700	2.01	0.74
LI225	2.50	0.49
LI350	1.96	0.14
LI480	2.02	0.45
LI620	2.06	0.47
LI700	2.30	0.61
KI225	1.99	0.56
KI350	2.00	0.08
KI480	2.00	0.23
KI620	2.00	0.21
KI700	2.58	0.74

2.2 Characterization techniques and analysis methods

2.2.1 Morphology- SEM

The scanning electron microscope uses the focused beam of high-energy electrons to generate various signals on the surface of solid specimens. The signals derived from the electron-sample interactions provide sample information, including external morphology (texture), chemical composition, and the crystalline structure and orientation of the sample materials. The collected data on a selected surface of the sample in most

applications and a two-dimensional image showing spatial variations on those properties will generate [45].

In conventional SEM technology, areas ranging from about 1 cm to 5 microns of width can be viewed in scan mode (magnification ranging from 20X to approximately 30,000X, a spatial resolution of 50 to 100 nm). This approach is instrumental in determining the chemical compositions (using EDX), crystal structure, and crystal guidelines. The SEM is also capable of analyzing selected areas in the sample. In this study, a high-resolution Scanning Electron Microscope (HR-SEM) Zeiss Merlin has been used to study the morphology of synthesized powder crystals. SEM images were developed by Dr. Valdek Mikli at the Tallinn University of Technology.

2.2.2 Elemental composition- EDX

Energy Dispersive X-ray analysis or energy dispersive X-ray microanalysis, this analytical method is used to analyze a sample elemental analysis or to characterize its chemical composition. It depends on a source of X-ray excitation and a sample interaction. In this study, the bulk composition of the synthesized powder crystals analyzed by the Energy Dispersive X-ray analysis was on done by HR-SEM Zeiss Merlin equipped with Bruker EDX-XFlash6/30 detector with an accelerating voltage of 20 kV. EDX measurements were performed by Dr. Valdek Mikli at the Tallinn University of Technology.

2.2.3 Phase analysis- Raman Spectroscopy

Raman spectroscopy is a non-destructive chemical analysis method that generates brief information about chemical structure, surface analysis, and heterointerfaces between the constituent layers of low-dimensional structures with laser light. Its analysis of the materials is based on the interaction between light and the chemical bonds in a material. Any molecules in gas, solid, or liquid interact with light; by that time, most of the photons will disperse or scattered at the same energy level in the form of incident photons. This can be defined as elastic scattering or Rayleigh scattering. Around one photon per 10 million will be scattered at a different frequency from the incident photon. This process is called inelastic dispersion, or Raman effect, named after a Noble Prize, awarded physicist Sir C.V. Raman. The Raman spectroscopy will be used to identify the chemical structure, phase analysis, intrinsic stress/strain contamination, and impurity of a material [26]. In this study, the Raman spectroscopic analysis was performed using a Horiba LabRAM HR800 micro- Raman system equipped with a cooled multichannel CCD detection system in the backscattering configuration with a spectral resolution better than 1 cm^{-1}. A YAG: Nd laser (wavelength λ=532 nm) was used for excitation for 100 seconds at room temperature.

3. RESULTS

3.1 Phase evolution in the system Cu-CdSe-Ge-Se in different salts at 225 °C

Figure 8 shows the SEM images of powder particles and corresponding cross-sections after holding the precursor materials at 225 °C for 1 week in different flux materials. Figure 8a shows powder particles synthesized in CdI_2. The particles have uneven shapes, particles are agglomerated, and the particle's surface is porous.

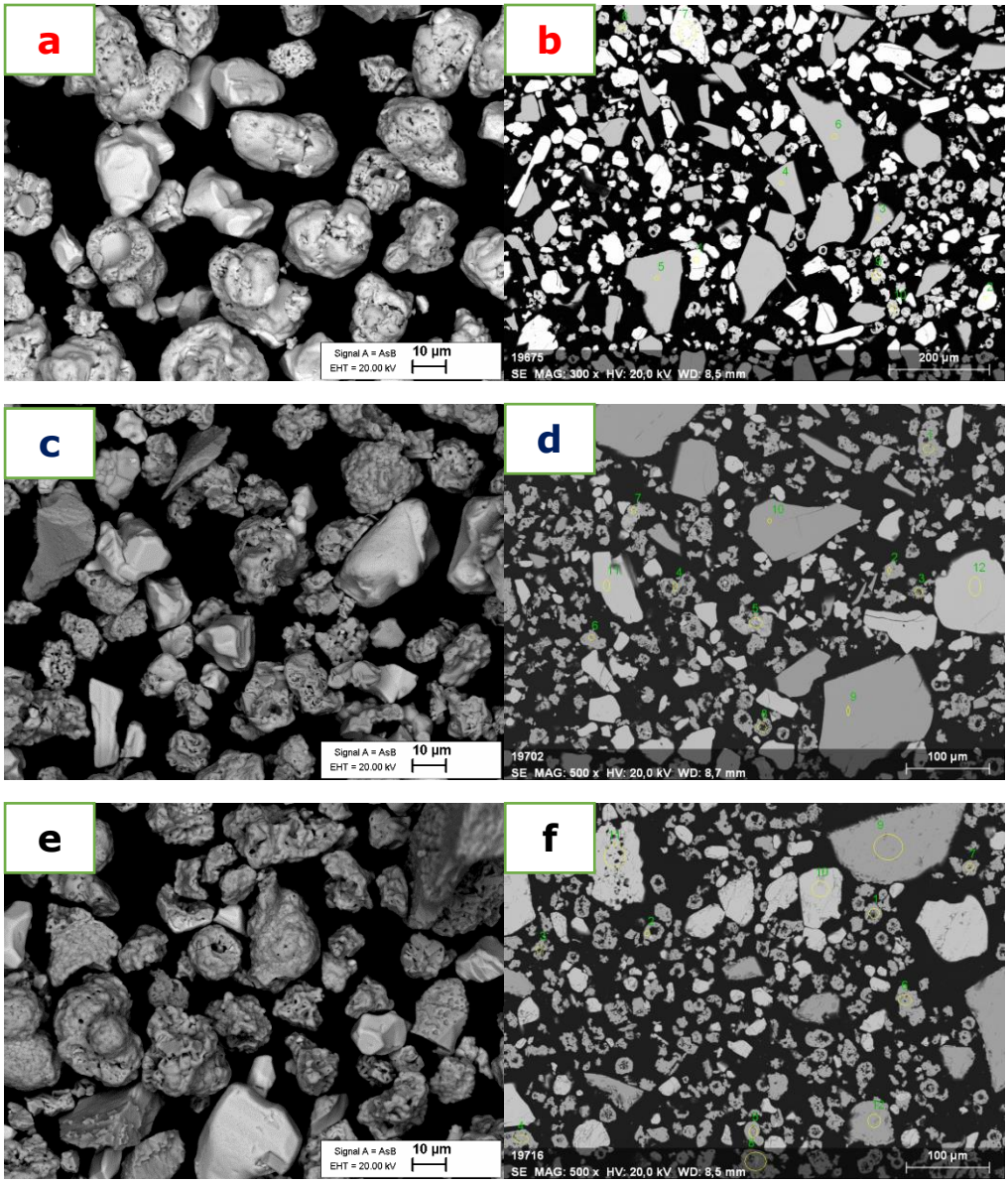

Figure 8: The SEM images of powder particles and corresponding cross-sections synthesized in different molten salts a, b) CdI_2, c, d) LiI, and e, f) in KI at temperatures 225 °C.

Energy Dispersive X-Ray Analysis (EDX) was used to characterize the elemental composition of formed powder particles. Figures 8b, d, f shows polished cross-sections of individual particles synthesized in CdI_2, LiI, and KI fluxes at 225 °C, respectively.

EDX analysis was done on some of the randomly chosen particles labeled in Figures 8b,d,f. According to the EDX results, there are mainly binary compounds CdSe (particles marked by 1, 2, and 7 in Figure 8b) and $CuSe_2$ (particles marked by 8, 9, and 10 in Figure 8b). and unreacted Ge (particles marked by 3, 4, 5, 6 in Figure 8b) in powder synthesized in CdI_2 flux. Figure 8c and d show powder particles synthesized in LiI. The particles have similar morphology to particles in CdI_2 flux. According to the EDX results, there are mainly binary compounds $CuSe_2$ (particles marked by 1, 2, 4, 5, and 6 in Figure 8d), CuSe (particles marked by 3 in Figure 8d), CdSe (particles marked by 11 and 12 in the Figure 8d) and unreacted Ge (particles marked by 9 and 10 in the Figure 8d).

Figure 8e and f show powder particles synthesized in KI. The particles have similar morphology to particles in the above-mentioned fluxes. According to the EDX results, there are mainly binary compounds $CuSe_2$ (particles marked by 1-8 in Figure 8f), CdSe (particles marked by 10 and 11 in Figure 8f), and unreacted Ge (particles marked by 9 and 12 in Figure 8f).

The phase composition of solid particles synthesized in different fluxes was also analyzed by Raman Spectroscopy. It has emerged as a practical technique for advanced characterization for different phases. Figures 9.1 and 9.2 show Raman spectra of powder particles synthesized in a) CdI_2, b) LiI and c) KI molten salts at temperature 225 °C.

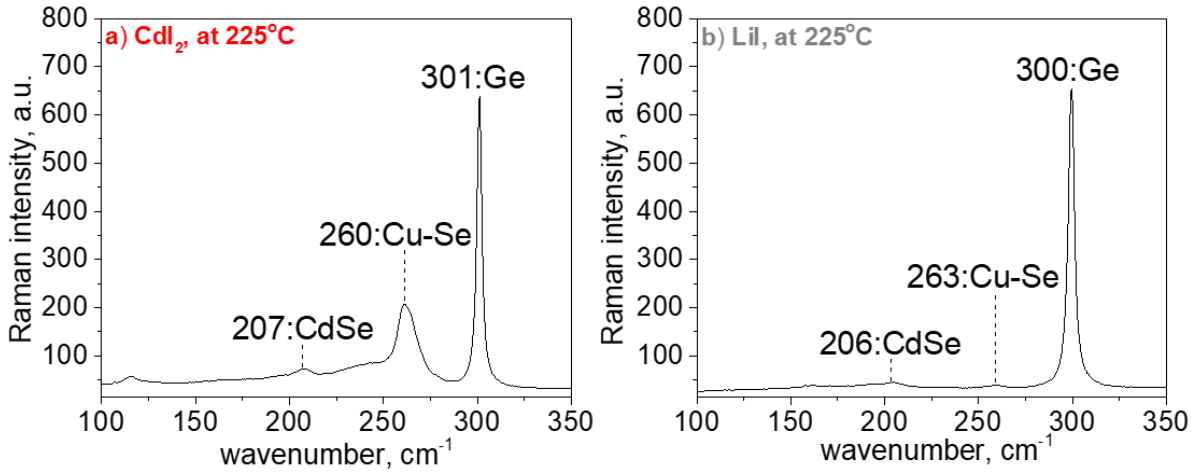

Figure 9.1: Raman spectra of powder particles synthesized in a) CdI_2 and b) LiI molten salts at temperature 225 °C.

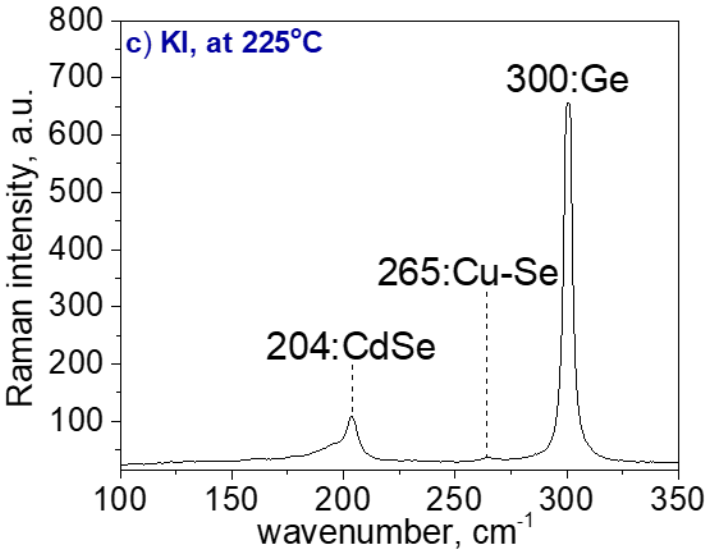

Figure 9.2: Raman spectra of powder particles synthesized in c) KI molten salt at temperature 225 °C.

The most intensive peak was observed with a little shift at 301 cm^{-1} for CdI_2 and at 300 cm^{-1} for LiI and KI synthesized particles. This peak is attributed to the crystalline Ge phase as Raman transverse optical (TO) mode [46]. The Raman peaks between 260- 265 cm^{-1} belong to binary Cu-Se compounds [47]. Raman peaks at 204-207 cm^{-1} correspond to the longitudinal optical (LO) and 2LO modes of the CdSe phase, respectively [9]. The small shift in peak position is depending on the used flux material.

3.2 Phase evolution in the system Cu-CdSe-Ge-Se in different salts at 350 °C

Figure 10 shows powder particles synthesized at a temperature of 350 °C in different molten salts (CdI_2, LiI and, KI). The particles synthesized in CdI_2 are smaller compare to particles grown in other molten salts.

The SEM images show that the big, rounded particles are formed in molten LiI and KI salts. Here also the crystals have an uneven shape, and the surface is porous.

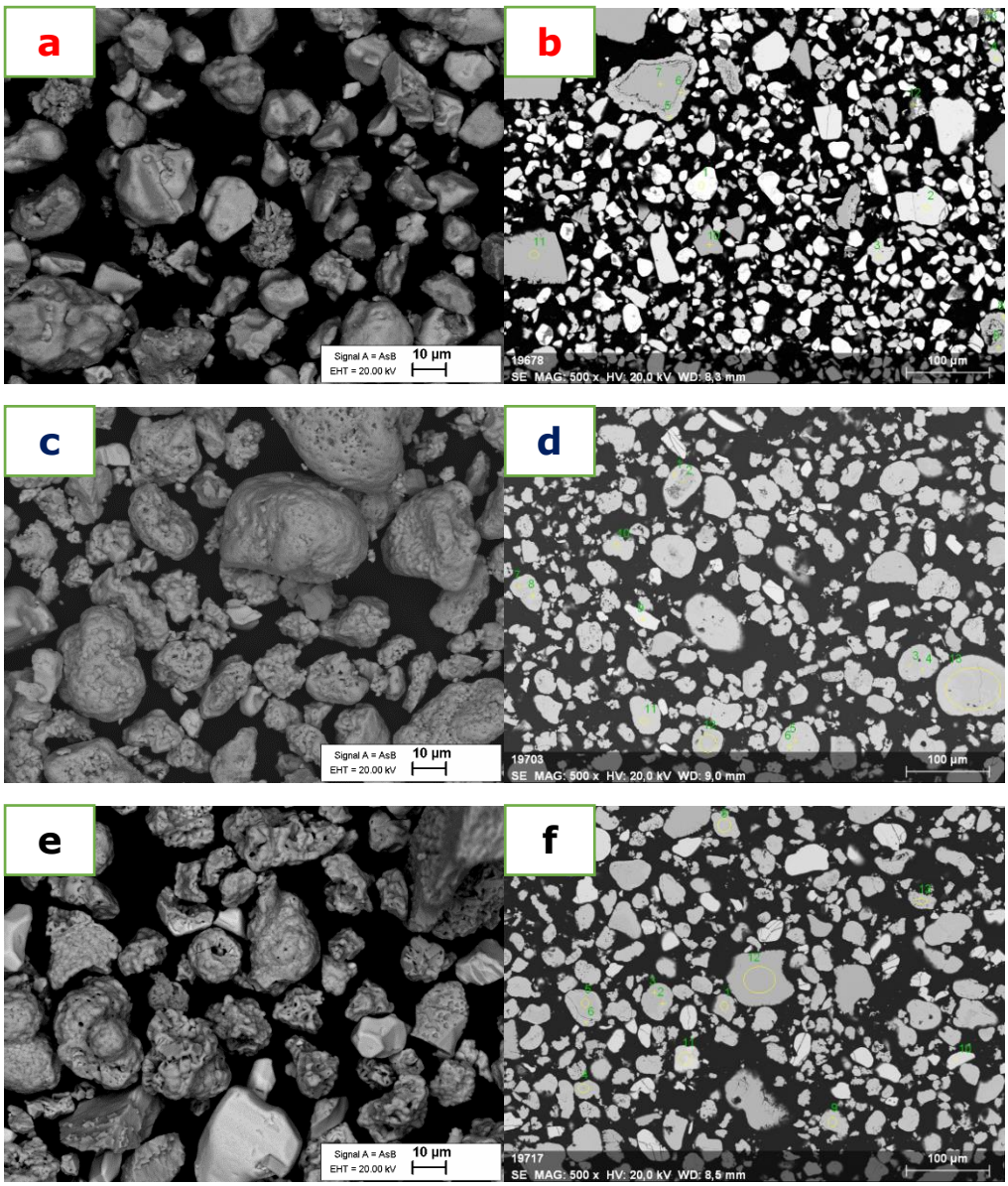

Figure 10: The SEM images of powder particles and corresponding cross-sections synthesized in different molten salts a, b) CdI_2, c, d) LiI, and e, f) in KI at temperatures 350 °C.

According to the phase diagram [48], $CuSe_2$ melts incongruently at 347° C to CuSe and a Se-rich liquid. CuSe reacts with $GeSe_9$ and forms ternary compound Cu_2GeSe_3 by following reaction [48]:

$$2\ CuSe(s) + GeSe_9\ (l) \rightarrow Cu_2GeSe_3 + 4\ Se_2\ (g)$$

According to EDX analysis, powder synthesized in CdI_2 at 350 °C contains still many different phases like a binary compounds $CuSe_2$ (particles marked by 3 and 4 in Figure 10b), CdSe (particles marked by 2 in Figure 10b), ternary Cu_2GeSe_3 (particles marked by 6 and 9 in Figure 10b), quaternary compound $Cu_2CdGeSe_4$ (particles marked by 1, 2, 5

and 8 in Figure 10b) and unreacted Ge (particles marked by 7, 10 and 11 in Figure 10b). At 350 °C formed quaternary phase $Cu_2CdGeSe_4$ particles are still with very inhomogeneous composition. The quaternary compound is formed by the following reaction:

$$Cu_2GeSe_3 + CdSe\ (s) \rightarrow Cu_2CdGeSe_4$$

According to EDX analysis, powder synthesized in LiI at 350 °C contains mainly ternary Cu_2GeSe_3 (particles marked by 3, 4, 5, 7, 12, and 13 in Figure 10d) and quaternary $Cu_2CdGeSe_4$ compounds (particles marked by 1, 6, 8, 10 and 11 in the Figure 10d) and some traces of unreacted CdSe (particle marked by 9 in the Figure 10d) and Ge (particle marked by 2 in the Figure 10d).

According to EDX analysis, powder synthesized in KI at 350 °C contains mainly ternary Cu_2GeSe_3 (particles marked by 3, 4, 5, and 7 in Figure 10f) and quaternary $Cu_2CdGeSe_4$ compounds (particles marked by 1, 2, 6, 9, and 13 in the Figure 10f) and some traces of unreacted CdSe (particle marked by 10 and 11 in the Figure 10f), $GeSe_2$ (particle marked by 8 in the Figure 10f). and Ge (particle marked by 12 in Figure 10f).

Nevertheless, the traces of the quaternary compound $Cu_2CdGeSe_4$ are already found in the monograins synthesized in KI. Figures 10b, d, f shows polished cross-sections of individual particles synthesized in CdI_2, LiI, and KI fluxes at 350 °C, respectively.

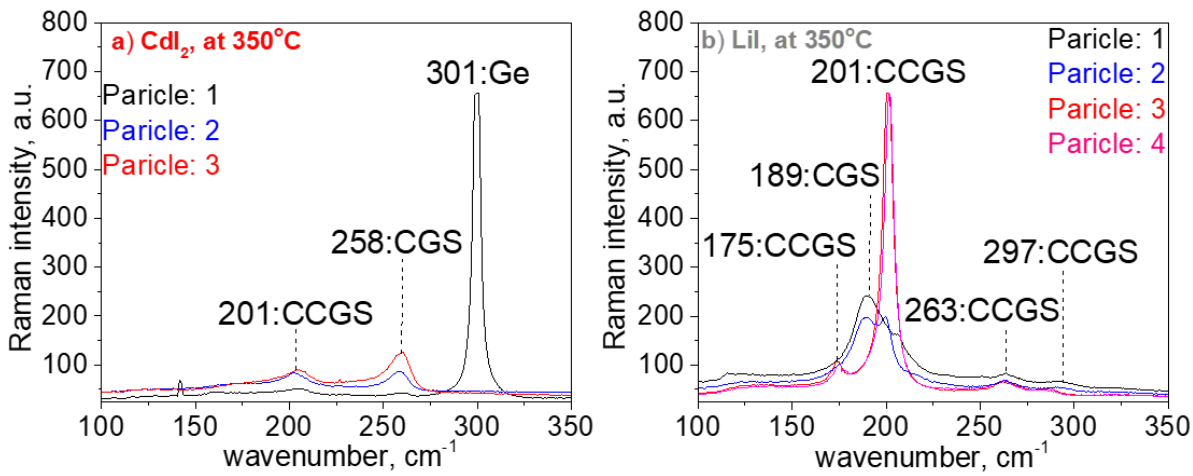

Figure 11.1: Raman spectra of powders synthesized in different molten salts a) CdI_2 and b) LiI at temperature 350 °C.

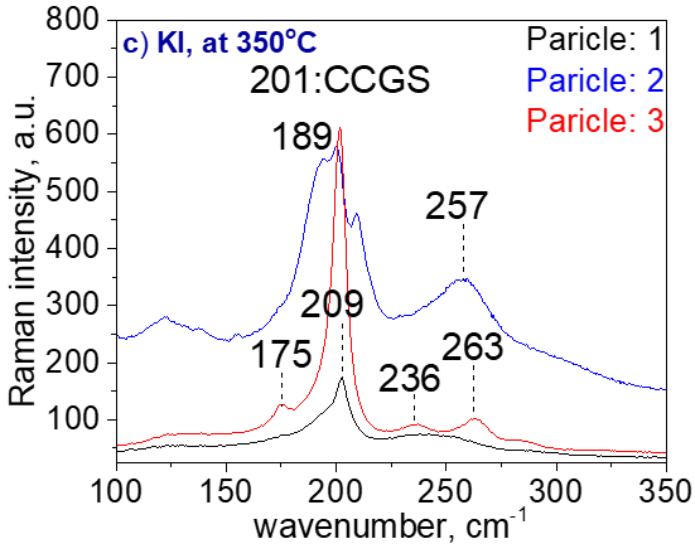

Figure 11.2: Raman spectra of powders synthesized in different molten salts c) KI at temperature 350 °C.

Raman Spectroscopy was also used to confirm the phase composition of powders synthesized in CdI_2, LiI and, KI flux materials at a temperature of 350 °C. Figures 11.1 and 11.2 illustrate the Raman peaks of phase composition of materials and confirm the existence of potential phases established.

For powder synthesized in CdI_2 at 350 °C, a strong peak at 301 cm^{-1} was observed. This belongs to Ge. Weak Raman peak at 201 cm^{-1} belongs to the quaternary $Cu_2CdGeSe_4$ phase [9]. In addition to them, ternary phase Cu_2GeSe_3 was detected at 258 cm^{-1} for powder synthesized in CdI_2 at 350 °C.

Raman spectra for powders synthesized in LiI and KI show the strongest peak at 201 cm^{-1}, which belongs to the quaternary $Cu_2CdGeSe_4$ compound. According to a study [9], it is a low-temperature tetragonal $Cu_2CdGeSe_4$ phase, which has other characteristic peaks at 175, 263, and 297 cm^{-1}. Raman mode at 189 cm^{-1} is signed to the A2 mode of the Cu_2GeSe_3 phase and other peaks are 209, 236, and 257 cm^{-1} [48].

3.3 Phase evolution in the system Cu-CdSe-Ge-Se in different salts at 480 °C

Figure 12 shows the SEM images of $Cu_2CdGeSe_4$ powder crystals synthesized in CdI_2, LiI and, KI molten salts at temperatures 480 °C. CdI_2 and LiI salts are in the liquid phase at 480 °C, this should enhance the crystal formation remarkable.

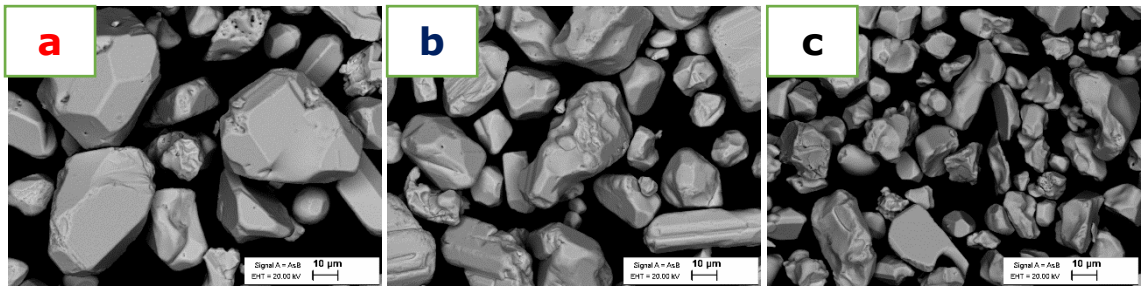

Figure 12: The SEM images of $Cu_2CdGeSe_4$ powder crystals synthesized in a) CdI_2, b) LiI and, c) KI molten salts at temperatures 480 °C.

SEM images confirm that the surface of the crystals starts becoming smoother and crystals are grown bigger because the dissolution is faster at higher temperatures. This explains the change in the direction of crystal growth is detected from this temperature (480 °C).

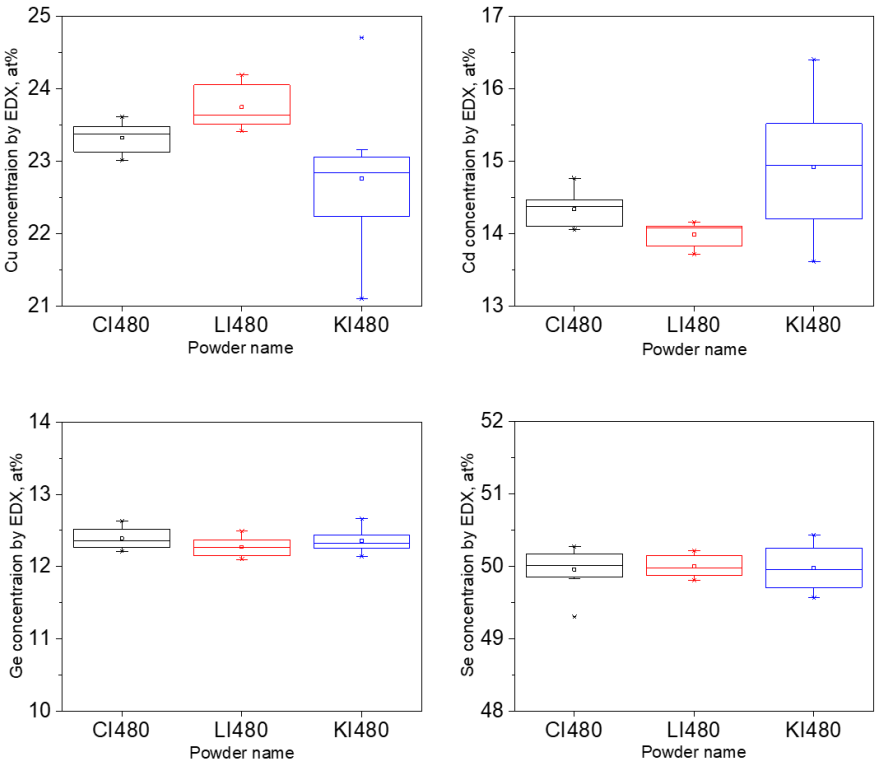

Figure 13: Boxplot of the composition of $Cu_2CdGeSe_4$ powder crystals synthesized in different molten salts (CdI_2, LiI and, KI) at temperatures 480 °C.

Compare to other low temperatures (225 and 350 °C) the monograin powders synthesized 480 °C clearly show the quaternary compound i.e., $Cu_2CdGeSe_4$ in all three molten salts (CdI_2, LiI and, KI) by EDX analysis.

Figure 13 illustrates the composition of individual elements (Cu, Cd, Ge, and Se) in $Cu_2CdGeSe_4$ crystals grown in different molten salts at 480 °C. The average Cu concentration is similar in crystals synthesized in CdI_2 and LiI fluxes by varying in the range 23.3-23.8 at%. $Cu_2CdGeSe_4$ crystals grown in KI have average Cu content is 22.8 at%. The average Cd concentration is similar in crystals synthesized in CdI_2 and KI fluxes by varying in the range 14.4-14.9 at%.

But fluctuation in Cd content in different crystals is largest for powder crystals synthesized in KI (Figure 13). Ge content is similar for all powders varying only in the range 12.3-12.4 at%. Table 4 describes the average composition of $Cu_2CdGeSe_4$ monograin powders synthesized at a temperature of 480 °C based on collected EDX data.

Table 4. The average composition of $Cu_2CdGeSe_4$ monograins synthesized in different fluxes at 480 °C. The average composition is calculated from EDX measurement data.

Sample name	**Cu, at%**	**Cd, at%**	**Ge, at%**	**Se, at%**	**[Cu]/ ([Cd]+[Ge])**	**[Cd]/[Ge]**
CI480	23.3	14.4	12.4	49.9	0.87	1.16
LI480	23.8	13.9	12.3	50.0	0.91	1.14
KI480	22.8	14.9	12.4	50.0	0.84	1.21

In conclusion, all powders synthesized in different fluxes at 480 °C are Cu-poor ([Cu]/([Cd]+[Ge]))<1 and Cd-rich ([Cd]/[Ge]>1). Among them, powder synthesized in LiI shows a little bit more Cu-rich and less Cd content compared to other flux materials and powder synthesized in KI contains less Cu and the highest concentration of Cd. At 480 °C, the most homogenous composition of $Cu_2CdGeSe_4$ powder was received in LiI flux.

Figure 14 compares the Raman scattering measurement of $Cu_2CdGeSe_4$ monograin powder synthesized in CdI_2, LiI and, KI molten flux materials at a temperature of 480 °C. The most intensive peak in the spectra belongs to the $Cu_2CdGeSe_4$ phase at 200-203 cm^{-1}. $Cu_2CdGeSe_4$ powders synthesized in CdI_2 and KI have a tetragonal structure with other characteristic peaks at 172-175, 262, and 265 cm^{-1}.

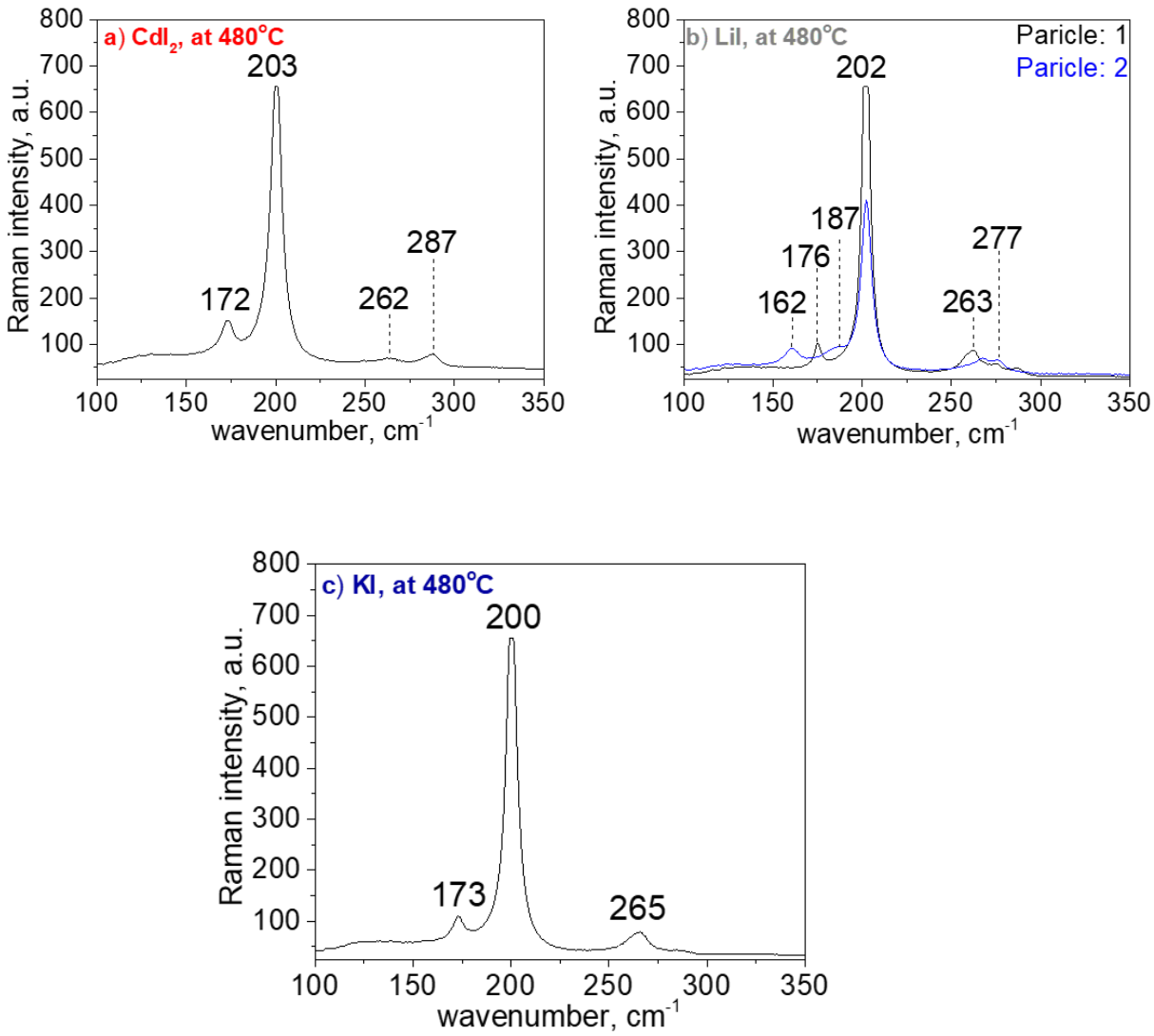

Figure 14: Raman spectra of $Cu_2CdGeSe_4$ powders in different molten salts (CdI_2, LiI and, KI) at temperatures 480 °C.

$Cu_2CdGeSe_4$ powders synthesized in LiI show two different Raman spectra. The most intensive peak in the spectra of $Cu_2CdGeSe_4$ is observed at 202 cm^{-1} and it is not depending on the phase structure. The additional characteristic Raman modes for the orthorhombic $Cu_2CdGeSe_4$ phase were detected at 162, 187, and 277 cm^{-1} (see Figure 14b) and for the tetragonal $Cu_2CdGeSe_4$ phase, the characteristic peaks were at 176 and 263 cm^{-1} [9].

3.4 Phase evolution in the system Cu-CdSe-Ge-Se in different salts at 620 °C

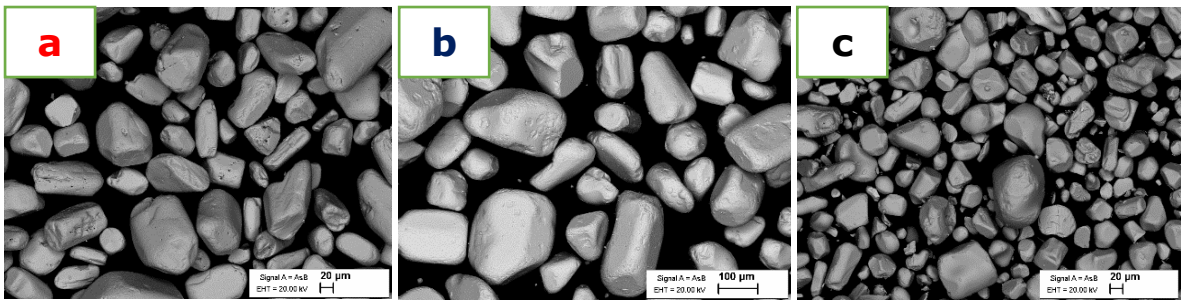

Figure 15: The SEM images of Cu2CdGeSe4 powder crystals synthesized in different molten salts (CdI2, LiI and, KI) at temperatures 620 °C.

Figure 15 shows the SEM images of $Cu_2CdGeSe_4$ powder crystals synthesized in a) CdI_2, b) LiI and, c) KI) molten salts at temperatures 620 °C. At temperature 620 ° C, major changes in grain growth were observed. At this stage, the grains were grown with rounded edges and more elongated with a smooth surface. From Figure 15b the monograins that were grown in LiI are much bigger than monograins grown in other flux materials (CdI_2 and KI). At this temperature, mainly the quaternary compound $Cu_2CdGeSe_4$ was identified by EDX analysis. However, there are still some traces of the binary CdSe phase in the powders grown in KI flux.

Results comparing homogeneity of elemental composition from different grains in $Cu_2CdGeSe_4$ powders synthesized in different fluxes at 620°C are shown as a box-plot diagram of statistical data in Figure 16. $Cu_2CdGeSe_4$ monograins grown in CdI_2 flux at 620 °C contain less Cu than monograins grown in LiI and KI flux. The average Cu content is 22.7 at% in $Cu_2CdGeSe_4$ monograins grown in CdI_2, but the Cu concentration is 23.5 and 23.9 at% for powders grown in LiI and KI, respectively. The crystals that have grown in CdI_2 do have a higher amount of Cd (15 at%), the lowest percentage of Cu and an almost equal amount of Ge and Se compare to crystals grown in LiI and KI fluxes. The concentration ratio of Cd/Ge=1.22 was observed for material grown in CdI_2 flux and it is much higher compare to materials grown in other flux materials.

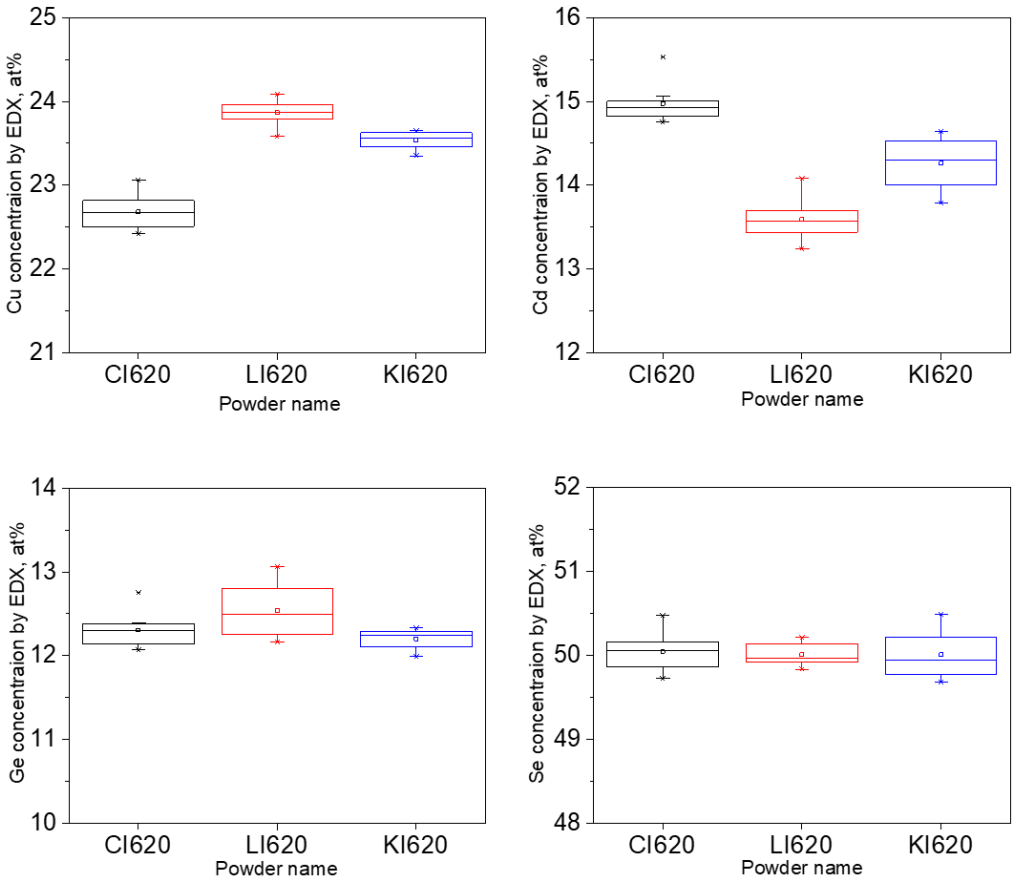

Figure 16: Boxplot of the composition of $Cu_2CdGeSe_4$ powder crystals synthesized in different molten salts (CdI_2, LiI and, KI) at temperatures 620 °C.

Table 5. The average composition of $Cu_2CdGeSe_4$ monograins synthesized in different fluxes at 620 °C. Composition is calculated from EDX measurement data.

Sample name	**Cu, at%**	**Cd, at%**	**Ge, at%**	**Se, at%**	**[Cu]/ ([Cd]+[Ge])**	**[Cd]/[Ge]**
CI620	22.7	15.0	12.3	50.0	0.83	1.22
LI620	23.9	13.6	12.5	50.0	0.91	1.08
KI620	23.5	14.3	12.2	50.0	0.89	1.17

The atomic percentage of all elements fluctuates more in $Cu_2CdGeSe_4$ powders synthesized in KI than the powders are grown in other flux materials (CdI_2 and LiI). It is probably due to lack of molten phase because CdI_2 melts at 387 °C and LiI at 446 °C, but KI is still solid at 620 °C (melting point is 681 °C).

In summary, all $Cu_2CdGeSe_4$ monograin powders synthesized at 620 °C have Cu-poor and Cd- rich composition. Compered to material grown in CdI_2 flux, the compositional ratio of Cu/(Cd+Ge) is higher in $Cu_2CdGeSe_4$ monograin powders grown in LiI and KI fluxes, 0.91 and 0.89, respectively (Table 5).

Raman spectra of $Cu_2CdGeSe_4$ powders grown in different molten salts (CdI_2, LiI and, KI) at temperatures 620 °C are shown in Figure 17. The most intensive peak at 202- 203 cm^{-1} corresponds to the quaternary $Cu_2CdGeSe_4$ phase. All other Raman peaks are detected at 160-162, 181, 240, 269, 270 and, 272 cm^{-1} not depending on the used flux material. It means that all $Cu_2CdGeSe_4$ powders synthesized at 620 °C crystallize in an orthorhombic structure.

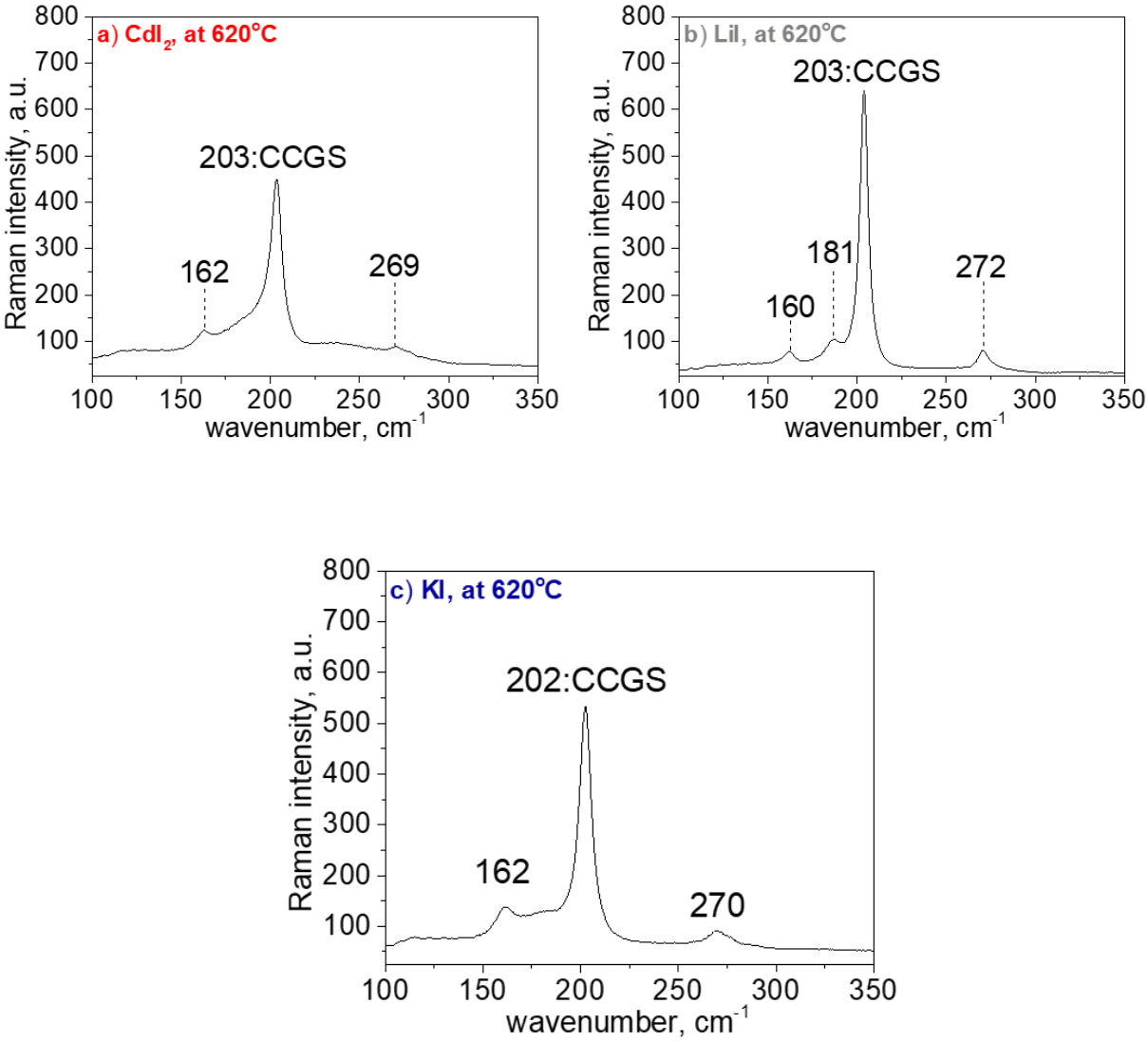

Figure 17: Raman spectra of $Cu_2CdGeSe_4$ synthesized in a) CdI_2, LiI, and c) KI molten salts at 620 °C.

3.5 Phase evolution in the system Cu-CdSe-Ge-Se in different salts at 700 °C

Figure 18 shows the SEM images of $Cu_2CdGeSe_4$ powder crystals synthesized in a) CdI_2, b) LiI and, c) KI molten salts at temperatures 700 °C. The crystals have slightly smooth edges, and the growth rate is much higher at temperature 700 °C. There were no traces of lumping or agglomeration of crystals observed. Each monograins are separated from the other. Visually the size variation was noticed in all flux materials. Some of the crystals grown in CdI_2 and KI are two times larger than others among them much smaller crystals can be noticed in KI.

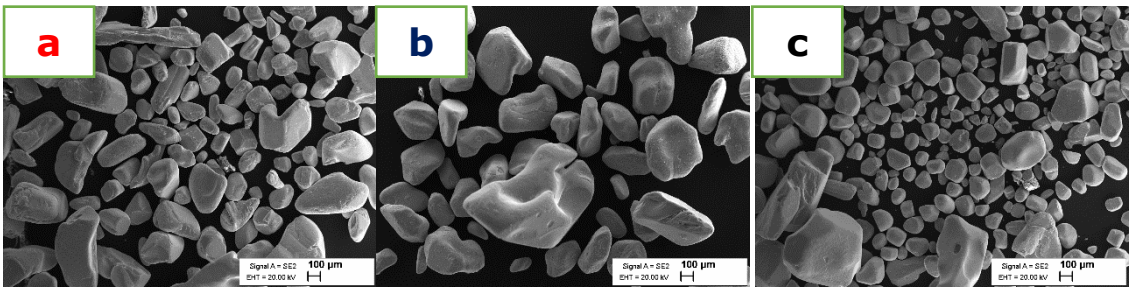

Figure 18 The SEM images of $Cu_2CdGeSe_4$ powder crystals synthesized in different molten salts (CdI_2, LiI and, KI) at temperatures 700 °C.

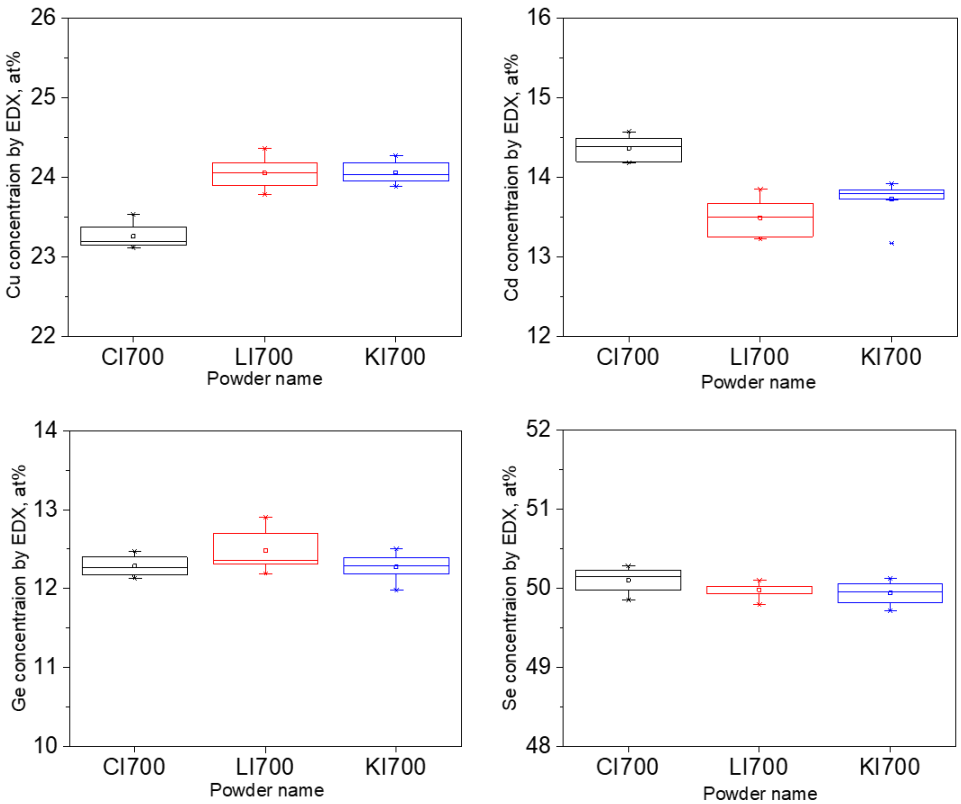

Figure 19: Boxplot of the composition of $Cu_2CdGeSe_4$ powder crystals synthesized in different molten salts (CdI_2, LiI and, KI) at temperatures 700 °C.

From the box plot (Figure 19), it is seen that the powders grown in LiI and KI fluxes at 700 °C have nearly the same elemental compositions (Table 6). Compered to powders synthesized in 620 °C, these materials contain slightly more Cu. But still, the ratio of Cu/(Cd+Ge) is 0.93 and Cd/Ge =1.08-1.12. Cd composition is slightly higher and Cu concentration is smaller for material synthesized in CdI_2. It is noticeable also in the compositional ratios of Cu/(Cd+Ge)=0.87 and Cd/Ge =1.17. The average concentration of Cu increased and Cd decreased in all materials synthesized at 700 °C compared to the lower temperature 620 °C.

Table 6. The average composition of $Cu_2CdGeSe_4$ monograins synthesized in different fluxes at 700 °C. Composition is calculated from EDX measurement data.

Sample name	Cu, at%	Cd, at%	Ge, at%	Se, at%	[Cu]/ ([Cd]+[Ge])	[Cd]/[Ge]
CI700	23.3	14.4	12.3	50.1	0.87	1.17
LI700	24.1	13.5	12.5	50.0	0.93	1.08
KI700	24.1	13.7	12.3	49.9	0.93	1.12

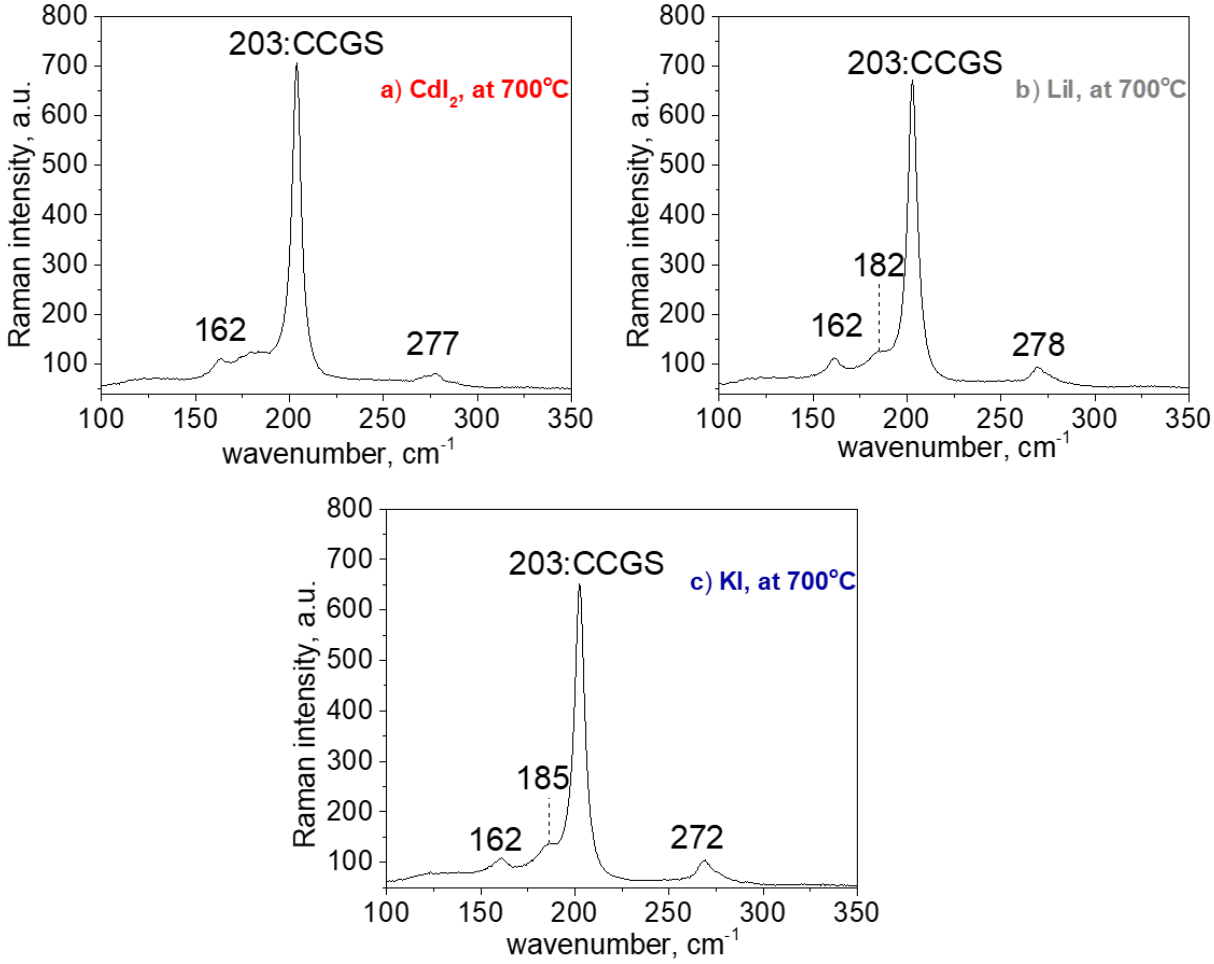

Figure 20: Raman spectra of $Cu_2CdGeSe_4$ synthesized in different molten salts (CdI_2, LiI and, KI) at temperatures 700 °C.

Raman spectra of $Cu_2CdGeSe_4$ powders grown in different molten salts (CdI_2, LiI and, KI) at temperatures 700 ^oC are shown in Figure 20. The most intensive peak at 203 cm^{-1} is identified for all powders not depending on used flux material. It corresponds to the quaternary $Cu_2CdGeSe_4$ phase. All other Raman peaks were also detected at 162, 182-185, 272-277 cm^{-1} not depending on the used flux material. It means that all $Cu_2CdGeSe_4$ powders synthesized at 700 ^oC crystallize in an orthorhombic structure.

SUMMARY

In this study, the phase evolution during the synthesis of $Cu_2CdGeSe_4$ monograin powders by molten salts method at different temperatures 225, 350, 480, 620, and 700 °C was investigated. The monograin powder was synthesized from high purity elemental metal powders Cu, Ge, and Se and binary powder CdSe. For fluxes, three different salts, CdI_2, LiI, and KI were used. The morphology, elemental composition, and phase analysis of synthesized crystals were investigated.

At 225 °C, according to SEM, EDX, and Raman analysis, Cu and Se precursors formed $CuSe_2$ independent of used flux materials, but CdSe and Ge precursors remained unchanged.

At 350 °C, according to EDX analysis, powder synthesized in CdI_2 contained still binary phases $CuSe_2$ and CdSe, new ternary phase Cu_2GeSe_3 was formed and some particles were already quaternary compound $Cu_2CdGeSe_4$. Powder particles synthesized in LiI and KI contained mainly ternary Cu_2GeSe_3 and quaternary $Cu_2CdGeSe_4$ compounds and some traces of unreacted CdSe and Ge. Raman analysis showed that formed $Cu_2CdGeSe_4$ quaternary compound particles had tetragonal structure independent of used flux.

At 480 °C, according to EDX and Raman analysis, all powders synthesized in different fluxes contained mainly quaternary compound $Cu_2CdGeSe_4$. All powders had Cu-poor ([Cu]/([Cd]+[Ge]))<1 and Cd-rich ([Cd]/[Ge]>1) composition. The most homogenous elemental composition of $Cu_2CdGeSe_4$ powder was received in LiI flux. Raman spectra showed that $Cu_2CdGeSe_4$ powders synthesized in CdI_2 and KI had characteristic peaks for tetragonal structure, but $Cu_2CdGeSe_4$ powder synthesized in LiI contained two different crystal structures – orthorhombic and tetragonal.

SEM images showed that the monograins that were grown in LiI at 620 °C were much bigger than monograins grown in other flux materials - CdI_2 and KI. At 620 °C, $Cu_2CdGeSe_4$ crystals that have grown in CdI_2 do have a higher amount of Cd (15 at%), the lowest percentage of Cu and an almost equal amount of Ge and Se compare to crystals grown in LiI and KI fluxes. The atomic percentage of all elements fluctuates more in $Cu_2CdGeSe_4$ powders synthesized in KI than the powders are grown in other flux materials (CdI_2 and LiI). Raman spectra of $Cu_2CdGeSe_4$ powders grown in different molten salts at temperatures 620 °C showed characteristic peaks for orthorhombic structure independent of used flux.

At 700 °C, the powders grown in LiI and KI fluxes had nearly the same elemental compositions. Cd content was slightly higher and Cu content was smaller for material

synthesized in CdI_2. But still, all powders had Cu-poor and Cd-rich compositions. According to Raman analysis, all $Cu_2CdGeSe_4$ powders synthesized at 700 °C crystallize in an orthorhombic structure.

In conclusion, the quaternary compound $Cu_2CdGeSe_4$ powders could be synthesized at temperature 480 °C and higher in all studied flux materials, but the homogenous composition and single-crystal structure of powders were observed at 620 °C and 700 °C.

LIST OF REFERENCES

[1] A. Luque and S. Hegedus, "Handbook of Photovoltaic Science and Engineering," .

[2] "Various Advantages and Examples of Solar Energy - Conserve Energy Future." https://www.conserve-energy-future.com/advantages_solarenergy.php (accessed May 12, 2021).

[3] M. Kaelin, D. Rudmann, and A. N. Tiwari, "Low cost processing of CIGS thin film solar cells," *Sol. Energy*, vol. 77, no. 6, pp. 749–756, Dec. 2004, doi: 10.1016/j.solener.2004.08.015.

[4] T. Wada, N. Kohara, S. Nishiwaki, and T. Negami, "Characterization of the Cu(In,Ga)Se_2/Mo interface in CIGS solar cells," *Thin Solid Films*, vol. 387, no. 1–2, pp. 118–122, May 2001, doi: 10.1016/S0040-6090(00)01846-0.

[5] L. M. Mansfield *et al.*, "Efficiency increased to 15.2% for ultra-thin Cu(In,Ga)Se_2 solar cells," *Prog. Photovoltaics Res. Appl.*, vol. 26, no. 11, pp. 949–954, Nov. 2018, doi: 10.1002/pip.3033.

[6] S. Ahmed, K. B. Reuter, O. Gunawan, L. Guo, L. T. Romankiw, and H. Deligianni, "A high efficiency electrodeposited Cu_2ZnSnS_4 solar cell," *Adv. Energy Mater.*, vol. 2, no. 2, pp. 253–259, Feb. 2012, doi: 10.1002/aenm.201100526.

[7] S. I. Swati, R. Matin, S. Bashar, and Z. H. Mahmood, "Experimental study of the optical properties of Cu_2ZnSnS_4 thin film absorber layer for solar cell application," in *Journal of Physics: Conference Series*, Sep. 2018, vol. 1086, no. 1, p. 12010, doi: 10.1088/1742-6596/1086/1/012010.

[8] J. Krustok *et al.*, "Observation of band gap fluctuations and carrier localization in $Cu_2CdGeSe_4$," *J. Phys. D. Appl. Phys.*, vol. 52, no. 28, p. 285102, May 2019, doi: 10.1088/1361-6463/ab1afd.

[9] M. Kauk-Kuusik *et al.*, "Study of $Cu_2CdGeSe_4$ monograin powders synthesized by molten salt method for photovoltaic applications," *Thin Solid Films*, vol. 666, pp. 15–19, Nov. 2018, doi: 10.1016/j.tsf.2018.09.025.

[10] A. Bosio, S. Pasini, and N. Romeo, "The history of photovoltaics with emphasis on CdTe solar cells and modules," *Coatings*, vol. 10, no. 4. MDPI AG, p. 344, Apr. 01, 2020, doi: 10.3390/coatings10040344.

[11] J. J. Loferski, "The first forty years: A brief history of the modern photovoltaic age," *Prog. Photovoltaics Res. Appl.*, vol. 1, no. 1, pp. 67–78, Jan. 1993, doi: 10.1002/pip.4670010109.

[12] T. Kato, "Cu(In,Ga)$(Se,S)_2$ solar cell research in Solar Frontier: Progress and current status," in *Japanese Journal of Applied Physics*, Apr. 2017, vol. 56, no. 4, p. 04CA02, doi: 10.7567/JJAP.56.04CA02.

[13] "First Solar Achieves Yet Another Cell Conversion Efficiency World Record – PES – Power & Energy Solutions." http://www.pes.eu.com/renewable-news/first-solar-achieves-yet-another-cell-conversion-efficiency-world-record/ (accessed May 12, 2021).

[14] "2019." https://www.solar-frontier.com/eng/news/2019/0117_press.html (accessed May 12, 2021).

[15] O. Vigil-Galán *et al.*, "Route towards low cost-high efficiency second generation solar cells: current status and perspectives," *J. Mater. Sci. Mater. Electron.*, vol. 26, no. 8, pp. 5562–5573, Aug. 2015, doi: 10.1007/s10854-014-2196-4.

[16] R. Fonoll-Rubio *et al.*, "Insights into interface and bulk defects in a high efficiency kesterite-based device," *Energy Environ. Sci.*, vol. 14, no. 1, pp. 507–523, Jan. 2021, doi: 10.1039/d0ee02004d.

[17] K. Ito, "Preface," *Copper Zinc Tin Sulfide-Based Thin Film Solar Cells*. wiley, pp. ix–x, Jan. 30, 2015, doi: 10.1002/9781118437865.

[18] E. Mellikov *et al.*, "Monograin materials for solar cells," *Sol. Energy Mater. Sol. Cells*, vol. 93, no. 1, pp. 65–68, Jan. 2009, doi: 10.1016/j.solmat.2008.04.018.

[19] "Monograin Layer Solar Cell Technology for Space Application - Issuu." https://issuu.com/eas-estonia/docs/estonian_space_technologies_phone_book_2020/s/11869700 (accessed May 12, 2021).

[20] S. Das, K. C. Mandal, and R. N. Bhattacharya, "Earth-Abundant $Cu_2ZnSn(S,Se)_4$ (CZTSSe) solar cells," in *Semiconductor Materials for Solar Photovoltaic Cells*, Springer International Publishing, 2015, pp. 25–74.

[21] C. Wang *et al.*, "Design of I_2-II-IV-VI_4 semiconductors through element substitution: The thermodynamic stability limit and chemical trend," *Chem. Mater.*, vol. 26, no. 11, pp. 3411–3417, Jun. 2014, doi: 10.1021/cm500598x.

[22] S. Giraldo *et al.*, "How small amounts of Ge modify the formation pathways and crystallization of kesterites," *Energy Environ. Sci.*, vol. 11, no. 3, pp. 582–593, Mar. 2018, doi: 10.1039/c7ee02318a.

[23] W. Wang *et al.*, "Device characteristics of CZTSSe thin-film solar cells with 12.6% efficiency," *Adv. Energy Mater.*, vol. 4, no. 7, p. 1301465, May 2014, doi: 10.1002/aenm.201301465.

[24] S. Giraldo, Z. Jehl, M. Placidi, V. Izquierdo-Roca, A. Pérez-Rodríguez, and E. Saucedo, "Progress and Perspectives of Thin Film Kesterite Photovoltaic Technology: A Critical Review," *Advanced Materials*, vol. 31, no. 16. Wiley-VCH Verlag, p. 1806692, Apr. 19, 2019, doi: 10.1002/adma.201806692.

[25] E. Mellikov *et al.*, "Growth of CZTS-Based Monograins and Their Application to Membrane Solar Cells," in *Copper Zinc Tin Sulfide-Based Thin-Film Solar Cells*, wiley, 2015, pp. 289–309.

[26] G. Q. Yao, H. S. Shen, E. D. Honig, R. Kershaw, K. Dwight, and A. Wold, "Preparation and characterization of the quaternary chalcogenides $Cu_2B(II)C(IV)X_4$ [B(II) = Zn, Cd; C(IV) = Si, Ge; X = S, Se]," *Solid State Ionics*, vol. 24, no. 3, pp. 249–252, Aug. 1987, doi: 10.1016/0167-2738(87)90166-4.

[27] L. Guen, W. S. Glaunsinger, and A. Wold, "Physical properties of the quarternary chalcogenides $Cu_2IBIICIVX_4$ (BII = Zn, Mn, Fe, Co; CIV = Si, Ge, Sn; X = S, Se),"

Mater. Res. Bull., vol. 14, no. 4, pp. 463–467, Apr. 1979, doi: 10.1016/0025-5408(79)90186-7.

[28] L. D. Gulay, Y. E. Romanyuk, and O. V. Parasyuk, "Crystal structures of low- and high-temperature modifications of $Cu_2CdGeSe_4$," *J. Alloys Compd.*, vol. 347, no. 1–2, pp. 193–197, Dec. 2002, doi: 10.1016/S0925-8388(02)00790-9.

[29] M. G. Brik, O. V. Parasyuk, G. L. Myronchuk, and I. V. Kityk, "Specific features of band structure and optical anisotropy of $Cu_2CdGeSe_4$ quaternary compounds," *Mater. Chem. Phys.*, vol. 147, no. 1–2, pp. 155–161, Sep. 2014, doi: 10.1016/j.matchemphys.2014.04.022.

[30] M. G. Brik, I. V. Kityk, O. V. Parasyuk, and G. L. Myronchuk, "Photoinduced features of energy bandgap in quaternary Cu_2CdGeS_4 crystals," *J. Phys. Condens. Matter*, vol. 25, no. 50, p. 505802, Dec. 2013, doi: 10.1088/0953-8984/25/50/505802.

[31] V. A. Ocheretova, O. V. Parasyuk, A. O. Fedorchuk, and O. Y. Khyzhun, "Electronic structure of $Cu_2CdGeSe_4$ single crystal as determined from X-ray spectroscopy data," *Mater. Chem. Phys.*, vol. 160, pp. 345–351, Jun. 2015, doi: 10.1016/j.matchemphys.2015.04.049.

[32] G. P. Bernardini and A. Catani, "The Cu-Se system," *Miner. Depos.*, vol. 3, no. 4, pp. 375–380, Dec. 1968, doi: 10.1007/BF00207529.

[33] O. F. Zmiy, I. A. Mishchenko, and I. D. Olekseyuk, "Phase equilibria in the quasi-ternary system Cu_2Se-CdSe-In_2Se_3," in *Journal of Alloys and Compounds*, Mar. 2004, vol. 367, no. 1–2, pp. 49–57, doi: 10.1016/j.jallcom.2003.08.011.

[34] H. Ipser, M. Gambino, and W. Schuster, "The germanium-selenium phase diagram," *Monatshefte für Chemie Chem. Mon.*, vol. 113, no. 4, pp. 389–398, Apr. 1982, doi: 10.1007/BF00799914.

[35] D. I. Bletskan, "Phase Equilibrium in the Systems AIV—BVI. Part 2. Systems Germanium—Chalcogen," *ChemInform*, vol. 37, no. 30, p. no-no, Jul. 2006, doi: 10.1002/chin.200630245.

[36] O. V. Marchuk, I. D. Olekseyuk, and A. G. Grebenyuk, "Phase equilibrium in the system Cu_2Se-HgSe-$GeSe_2$," *J. Alloys Compd.*, vol. 457, no. 1–2, pp. 337–343, Jun. 2008, doi: 10.1016/j.jallcom.2007.03.076.

[37] L. V. Piskach, O. V. Parasyuk, and Y. E. Romanyuk, "Phase equilibria in the quasi-binary Cu_2GeS_3/Se_3/-CdS/Se/ systems," *J. Alloys Compd.*, vol. 299, no. 1–2, pp. 227–231, Mar. 2000, doi: 10.1016/S0925-8388(99)00797-5.

[38] H. Matsushita, T. Maeda, A. Katsui, and T. Takizawa, "Thermal analysis and synthesis from the melts of Cu-based quaternary compounds Cu-III-IV-VI_4 and Cu_2-II-IV-VI_4 (II = Zn, Cd; III = Ga, In; IV = Ge, Sn; VI = Se)," *J. Cryst. Growth*, vol. 208, no. 1, pp. 416–422, Jan. 2000, doi: 10.1016/S0022-0248(99)00468-6.

[39] X. Li *et al.*, "Effect of absorber surface modification on the optoelectronic properties of $Cu_2CdGeSe_4$ solar cells.," *Thin Solid Films*, vol. 697, p. 137822, Mar. 2020, doi: 10.1016/j.tsf.2020.137822.

[40] Melting Point of Common Metals, Alloys, & Other Materials. (2021). American Elements: The Materials Science Company. https://www.americanelements.com/meltingpoint.html

[41] Cadmium Selenide. (2017, June 13). American Elements. https://www.americanelements.com/cadmium-selenide-1306-24-7

[42] Cadmium Iodide. (2017, June 13). American Elements. https://www.americanelements.com/cadmium-iodide-7790-80-9

[43] "Lithium iodide | LiI - PubChem." https://pubchem.ncbi.nlm.nih.gov/compound/Lithium-iodide (accessed May 12, 2021).

[44] Potassium Iodate-Iodide. (2017, June 13). American Elements. https://www.americanelements.com/potassium-iodate-iodide

[45] "Scanning Electron Microscopy (SEM)." https://serc.carleton.edu/research_education/geochemsheets/techniques/SEM.html (accessed May 12, 2021).

[46] G. X. Wang, M. S. Park, H. K. Liu, D. Wexler, and J. Chen, "Synthesis and characterization of one-dimensional CdSe nanostructures," Appl. Phys. Lett., vol. 88, no. 19, p. 193115, May 2006, doi: 10.1063/1.2202725.

[47] B. M. Palve, V. S. Kadam, C. V. Jagtap, S. R. Jadkar, and H. M. Pathan, "A simple chemical route to synthesis the CuSe and CuS counter electrodes for titanium oxide based quantum dot solar cells," *J. Mater. Sci. Mater. Electron.*, vol. 28, no. 19, pp. 14394–14401, Oct. 2017, doi: 10.1007/s10854-017-7300-0.

[48] G. Marcano *et al.*, "Raman scattering and X-ray diffraction study in Cu_2GeSe_3," *Solid State Commun.*, vol. 146, no. 1–2, pp. 65–68, Apr. 2008, doi: 10.1016/j.ssc.2008.01.018.